# Structural analysis of carbon fiber-epoxy composite surfaces with polar stacking sequences

*Daniel Sasser*

A thesis submitted in partial fulfillment of the requirements for the degree of

Master's of Science in Mechanical Engineering

*University of Washington*
2015

Committee:

Mark Tuttle

Nathan Sniadecki

Mamidala Ramulu

Program Authorized to Offer Degree:

Mechanical Engineering

©Copyright 2015

Daniel Sasser

University of Washington

# Abstract

## Structural analysis of carbon fiber-epoxy composite surfaces with polar stacking sequences

Daniel Edward Sasser

Chair of the Supervisory Committee:

Professor Mark Tuttle

Mechanical Engineering

In this study, a new method of constructing graphite-epoxy carbon fiber structures is examined. The method studied consists of placing small strips of carbon fiber pre-preg into the desired mold such that fibers emanate outward from one or more poles. The goals of this study were to (1) construct a flat panel and predict the behavior of a simple structure with a polar stacking sequence, (2) determine if a hemispherical dome with polar lay-up will buckle during cooling using ANSYS ACP, (3) predict the strains and displacements within the dome due to pressurization using ANSYS ACP, (4) measure strains on the surface of the pressurized dome with polar lay-up using resistance strain gauges, fiber optic strain gauges, and digital image correlation, and (5) compare the measured and predicted strains. During this study, a methodology for constructing panels with polar stacking sequences was developed and a method for modeling the panels with polar stacking sequences was created using ANSYS ACP. Additionally, this method was applied to hemispherical domes using ANSYS ACP. By using an eigenvalue analysis to analyze the panels and dome, it was determined whether or not they structure would buckle. It was determined that both one and two pole panels would buckle due to cooling from the elevated cure temperature and the dome would not buckle. The strains measured by the resistance strain gauges

and fiber optic gauge were compared to a standard classic lamination theory calculation and to the predictions made by the analyses performed in ANSYS ACP. The predicted and measured strains followed the same trends at all latitudes examined and were well captured by the ANSYS model. Additionally, the strain field captured by digital image correlation techniques agreed enveloped the predicted strain field from the ANSYS model. The digital image correlation techniques are subject to a significant amount of noise which made direct comparison of the scales difficult, however the gradients in the measured strain field were reflected in the ANSYS model.

# Table of Contents

## Table of Figures

# Introduction

## Background

Carbon fiber/epoxy composites have become more common in commercial applications over the last few decades as technology and analysis techniques improve, particularly in the aerospace, automobile, and marine industries. Composites are used because they can reduce weight while maintaining or even increasing the strength of some components. Many parts used in a wide range of structures are manufactured with curved surfaces and edges. It can be very difficult to manufacture stable curves and other non-planar surfaces using composites because of the thermomechanical nature of the thin sheets used to produce composite structures.

Since carbon fiber composites rely on the highly directional strengths of the fibers, having fibers misaligned or off-axis is detrimental to the overall laminate strength and stiffness of the part. Predicting these laminate properties can also be very difficult because of the misalignment of fibers across curved surfaces from draping the fabric over the mold used to create the part. There are some specialty fabrics and weaves designed to have improved drapability, however some misalignment is unavoidable. Current methods of certifying laminate properties for aerospace applications rely heavily on experimental testing initially and confirmed with finite element analysis. Once the initial part and methods have been verified, follow up parts and methods using similar principals can be verified with just finite element simulations.

One such part used frequently, in a wide range of industries, is a pressure vessel. For everyday use such as propane tanks for backyard grills, the weight considerations are negligible so long as the pressure vessel will not rupture. In aerospace use, shaving every possible pound off is critical and so composite pressure vessels are commonly used. NASA and many commercial companies (such as Composite Technology Development) have dedicated extensive research efforts towards developing different methods for manufacturing and certifying composite pressure vessels for use in space for both satellites and shuttles.

## Motivation

Creating a lighter pressure vessel or any other curved surface, such as the nose of an aircraft, the leading edge of a wing, or the fuselage, is desirable for aerospace uses. Additionally, using less material and ultimately decreasing the price of the component is beneficial. Typical pressure vessels are formed metallic tanks, composite overwrapped vessels with an inner liner, and fiber reinforced vessels without an inner liner [21]. Composite pressure vessels often are made using filament winding techniques. Composite pressure vessels have a significant weight advantage over all-metal vessels, however they are much more complicated and require unique design, manufacturing, and certification requirements [14]. An inner liner is usually necessary in a composite pressure vessel because microcracks form in the resin matrix of the composite which leads to leakage and ultimately failure of pressure vessels. However, some pressure vessels have been developed that work without an inner liner because they utilize a special resin system that is designed to be resistant to microcracking and thus leakage. Inner liners are typically made of metal or plastic, but do not contribute significantly to the material properties since it is mainly just to contain the fluid inside. Historically, most components of airplanes were made of metal, especially those with surfaces exposed to the outside air during flight. Now, airplanes such as the 787 are largely made with composite structures made in a variety of different ways with as many different lay-ups.

Since a higher specific strength (strength per unit weight) results in a light component, it is of interest to develop new methods of manufacturing composites. A typical method for creating both spherical and cylindrical composite structures is to use a filament winding technique to wrap tows around a formed liner. The fibers are typically wound in both the longitudinal (helical) and circumferential (hoop) direction on cylinders and around all directions on spherical parts. This results in a start and end point for the various tows based on the length of the spool of fibers used for wrapping (typically more than one end point unless the entire wrap is done on one spool).

On a wrapped structure, it is typically assumed that the endpoints have little effect on the overall laminate properties, however utilizing the endpoints and knowing exactly how they affect the properties could lead to reducing the weight and material of the structure. This led to the idea of a polar lay-up that involves fibers radiating outward from a series of points over the surface of a hemisphere (similar to lines of longitude on a globe). This method decreases the misalignment of fibers due to draping unidirectional or woven plies over curved surfaces, however, the method of manufacturing these polar lay-ups can lead to incredibly complicated and time intensive lay-ups. Previous to this study, several hemispherical domes were constructed using this polar method and it was shown that they can be produced, however it requires a significant amount of work.

## Objectives and Tasks

The objective of this study was to determine if the polar lay-up method for pressure vessels can be accurately modeled in the finite element composite package ANSYS ACP. Since several domes were previously produced and studied [previous work], the intent was to further study this lay-up and determine if ANSYS ACP can predict the strains caused by pressuring a dome accurately. The primary tasks involved in this were:

Task 1: Construct a flat panel using a polar lay-up with fibers radiating outward from one or more points and predict the behavior of this simple structure using ANSYS ACP.

Task 2: Determine if the hemispherical dome with polar lay-up will buckle (i.e., deform in a non-uniform manner) during cooldown following cure at an elevated temperature using ANSYS ACP.

Task 3: Predict the strains and displacements within the hemispherical dome due to pressurization using ANSYS ACP.

Task 4: Measure strains on the surface of the pressurized hemispherical dome with polar lay-up using standard resistance strain gauges, fiber optic strain gauges, and digital image correlation (DIC).

Task 5: Compare predicted and measured strains.

## Literature Review

Typical methods of manufacturing composite structures include hand lay-up, bag molding processes, resin transfer molding, filament winding, pultrusion, and preformed molding. This study utilized hand lay-up techniques for constructing composite parts. To produce the composite structures studied here, carbon fiber/epoxy pre-preg from Toray was used and placed by hand into the appropriate shape. [1] discusses many of the different methods for constructing composite structures, including hand lay-up with pre-preg.

### Finite Element Analysis

Modern finite element analysis methods are used predict the loads, stresses, strains, and deformed geometries involved in products from aerospace structures to household goods. The usual process followed is to create a 3D model of the structure to be analyzed, apply an element type and material properties, mesh the geometry, and apply any loading conditions. The additional step performed for composites is to specify the stacking sequence or lay-up of the structure to be analyzed. This process is typical for all types of analyses and thermal loading can also be analyzed using these same techniques. The University of Alberta website (http://www.mece.ualberta.ca/tutorials/ansys/) was used extensively as the baseline for the analyses conducted in this study.

### Digital Image Correlation

Digital Image Correlation (DIC) is a technique for measuring displacements, shape, or motion on the surface of a part by using one or more cameras. The surface of the part is covered with a non-repetitive speckling pattern with high contrast. While the test is being performed, digital camera(s) is/are used to capture images of the part over set time intervals. With one camera, only in plane displacements can be captured and if two are used, the surface of the part can be observed in three dimensions.

DIC works by taking the images captured throughout the test and processing them using software that compares each image to a reference image. The software calculates how far a small (unique) grouping of speckles has been displaced in each image. Once all of the small groupings have been analyzed, the displacement field on the surface of the part is fully captured. Once the displacement is known, the strain can be determined by the software simply by taking the derivative of the displacements. DIC cannot be used to calculate through thickness displacements due to the cameras only being able to capture images of the surface.

The speckled pattern is ideally non-repetitive, isotropic, uniformly sized, and high contrast [13]. In order for each small grouping to be unique, the speckling pattern must not repeat itself on the surface of the part. The speckling should be isotropic so that there is no directionality to the results (the pattern must not be directional). Large speckles will cause de-featuring of the analyses and smaller speckles will cause blurring, therefore the speckles must be uniform ideally. And finally the speckles should contrast well in order to capture the difference between the speckles as sharply as possible. The method used in this study was to spray the surface of the parts with white spray paint and then use black spray paint to speckle the surface (details are discussed in the Methods section below). The ideal speckle size is about 3-5 pixels wide in the images captured by the DIC cameras [13].

When setting up the software to process the captured images, several parameters must be adjusted and may have large impacts on results. As mentioned previously, the software tracks small groups of speckles that are called subsets. The subset size is one of the parameters that must be specified by the user. The smallest subset size used in this study was 35 by 35 pixels however some of the images captured of the dome required larger subset sizes due to the resolution of the speckles on the surface. The subset size should be chosen such that each subset is unique [15]. Around the edges of the image, the displacements are inaccurate within one half of the subset size of the edge due to the nature of the correlation process, however larger subset sizes result in higher accuracy for tracking each subset. The second parameter used in the software is step size. This is the number of pixels the software increments before creating a second subset. This implies that the subsets actually overlap more or less based on the size of the subset and the size of the step parameter. Increasing the size of the step results in faster correlation of the images and smoother strain results, however the spatial resolution is negatively affected, particularly in regions with high strain gradients. The final major parameter is the filter size. The strains calculated from the displacements are filtered by the software and if this is not chosen correctly, the results can be inaccurate, again, particularly in areas with high strain gradients.

## Unsymmetric Laminates

Many laminates with unsymmetric stacking sequences exhibit warping after cooling to room temperature from cure temperatures. Of these laminates, many of them also have several equilibrium states [8]. M. W. Hyer has done a large amount of research into unsymmetric laminates and most of the research done on unsymmetric laminates is based off his original work, [14 and 15]. A theoretical methodology to predict the configuration of the cooled unsymmetric laminates with $(-\theta_4/ \theta_4)_T$, $((90-\theta)_4/ \theta_4)_T$, and $((\theta-90)_4/ \theta_4)_T$ stacking sequences is given in [8]. Hyer and Dano further state that using any FEA code to run unsymmetric panel analyses can be very tedious and time consuming compared to using the theory developed in their research, especially when studying panels with fiber angles other than 0 and 90 degrees. In [14] Hyer discusses thin unsymmetric laminates and how they diverge from the saddle shape predicted by CLT. It elaborates that as a $[0_4/90_4]$ panel is cooled, the shape is dependent upon the thickness of the panel. After a certain point, the thicker panels cool into the saddle shape predicted by

CLT, but thin panels take on a similar shape to a right cylinder. The paper goes on to explain that the thickness-to-length ratio and width-to-length ratios of the laminate governs the shape developed by the panel during the cooling process.

# Methods

## Material Properties

Material properties were given in the data sheet for the T800H series fiber with 3900 series resin from the Toray Company. To confirm that the materials used had similar magnitudes to the material properties provided by the data sheet, the relevant laminate properties were determined via the methods outlined in the ASTM D3039 test standard utilizing an Instron Tensile Testing Machine Model 5585H test machine. The strain gauges used were M-M C2A-06-125WW-350 standard resistance strain gauges and the tests were performed on rectangular tensile coupons with the following stacking sequences: $[0]_8$, $[90]_{16}$, and $[45_2/-45_2]_s$. The $[0]_8$ specimen was used to calculate the elastic modulus ($\varepsilon_{11}$) in the fiber direction and the Poisson's ratio between the fibers and epoxy ($\nu_{12}$). The $[90]_{16}$ coupon was used to calculate the elastic modulus ($\varepsilon_{22}$) in the epoxy direction. The $[45_2/-45_2]_s$ coupon was used to calculate the shear modulus ($G_{12}$). The second and third stacking sequences were done with one inch by twelve inch tensile coupons and the first coupon was a half inch by twelve inches long. The specimens were not tested to failure because the strengths were unnecessary.

## Studies of Flat Plates Produced with Polar Stacking Sequences

### Geometry and Production

The first step in conducting the analyses of laminates with polar stacking sequences was attempting to create flat plates. The final panel geometry to be examined was a twelve inch by six inch panel with different pole locations, however each panel was made up of twelve plies. Several panels were constructed in order to test different methods of constructing the panels and the effect of pole location. Each panel was constructed using triangles that occupied 10 degrees of a circle, but the base and height of the triangles were not constant. The triangles were cut out using a MultiCam 700 model fabric cutter and one panel required about 432 triangles.

A typical process for curing these panels was to vacuum bag the panel and use an autoclave to cure it. The typical vacuum bagging process included a metal caul plate on the bottom, a layer of release ply, the composite panel, a layer of peel ply, then bleeder material, and finally a vacuum bag on top to seal it all in. The vacuum bag was sealed to the caul plate on bottom with yellow vacuum bag tacky tape with special care to keep everything else (including thermal tape and rogue fibers) out from under the tacky tape. The last component of the vacuum bagging process was the pressure inlet which needed to be placed off of the part, but inside the bag. The pressure inlet was made up of two parts, a small disc-like receptor and the actual pressure valve connected to the pressure line. The receptor had to be inside of the vacuum bag, on the surface, so that the bag could be cut slightly and have the pressure valve seated into the receptor.

The first panel was constructed with one pole in the center of the panel and each triangle had a height of six inches and base of one inch. To build the panel, a square piece of peel ply was taped onto a table, as seen in Figure 1. Each triangle was placed by hand such that the tips of the triangles met in the center. One challenge of this method was to get the tips to all meet in the center without overlapping and this was exacerbated by the fabric cutter slightly dragging on the fibers and making the edges of the triangles slightly off. Once all of the triangles in one layer were placed around in a circle, the next layer was placed on top of the first with the edges slightly overlapping the below layer. The whole lay-up was transferred to a caul plate and the plate was vacuum-bagged (according to the defined procedure above) and placed in a heated press and left to cure according to the cure cycle supplied in the material data sheet.

The panel cooled to room temperature and was removed from the hot press. The cooled panel adopted a shallow conical shape, shown in Figure 2, presumably due to thermal buckling caused by residual thermal stresses. After constructing the first panel, it was determined that it would not be sufficient for test purposes and the two pole panels were constructed to investigate if any panels constructed with polar stacking sequences would cure without buckling.

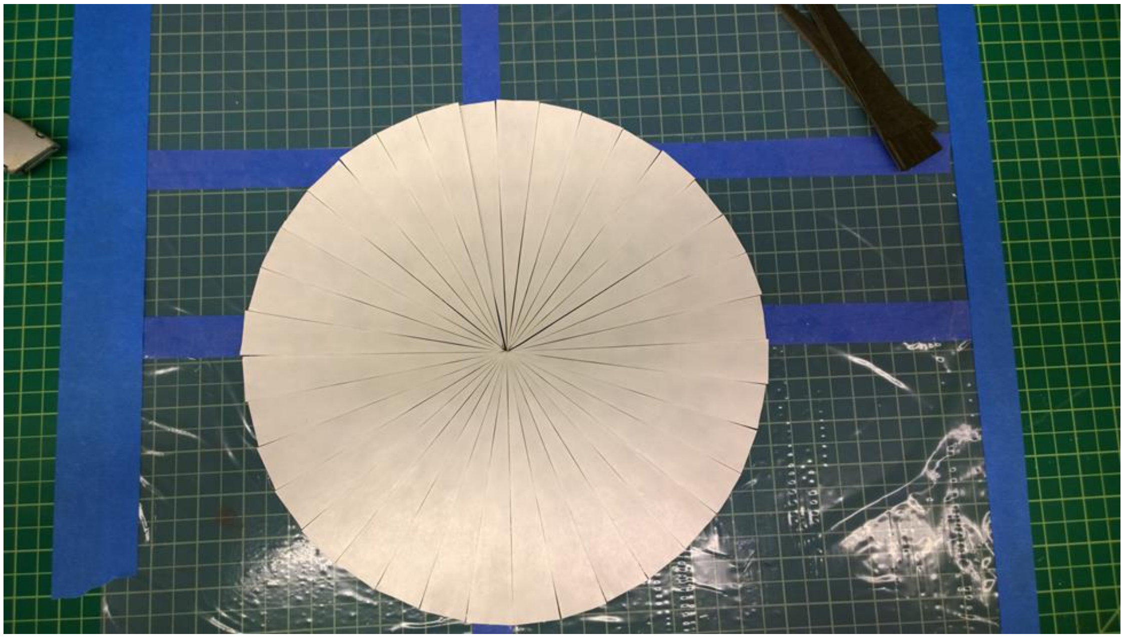

**FIGURE 1: PRECISION TABLE AND ONE-POLE LAYUP**

FIGURE 2: SHALLOW CONICAL SHAPE OF ONE-POLE PANEL AFTER CURE

At each pole location, the fibers in that ply are discontinuous and at the pole exactly, in a perfect world, there are no fibers. However, due to human error, there was some overlap of the tips of the triangles at the poles. This would be impossible to completely capture in an FEA model. Additionally, there was some overlap of the triangles sides as they were laid up around the panel. Again, in an ideal world each triangle would fit perfectly side by and the final triangle added to the lay-up would fit perfectly, however due to rounding error and some human error in placement, overlap and small gaps between the edges were inevitable. Additionally, the edges of the triangles were not always perfectly straight despite being cut on a CNC fabric cutting machine. This was most likely caused by a dull blade dragging the fabric partially. This was mitigated somewhat by taping the fabric onto the table before using the cutter, however it did not eliminate the problem.

The second panel was constructed with two poles in the panel. The first pole was at coordinates (0,3) and the second pole was at coordinates (0,-3). The origin (0,0) located at the center of the plate and the twelve inch edge parallel to the y-axis. The stacking sequence defined for this panel was $[(0,3)_3/(0,-3)_3]_{ss}$ which was defined to be three plies originating radially outward from (0,3), then three plies originating radially from (0,-3), and then mirrored for symmetry.

For this panel, rectangles eighteen inches long were cut out of pre-preg, stacked into three ply thick rectangular laminates, and then the triangles were cut out on the same fabric cutter. This resulted in a shorter amount of time needed to construct the panel and made it easier to stack the triangles. Once the triangles were cut, a piece of peel ply was taped down onto a precision cutting mat with one inch grid lines as shown in Figure 3. One problem with this stacking sequence was how to locate the poles once the first layer was down. In order to properly locate the poles, a piece of painters plastic was cut into an 'L' shape as shown in Figure 4. In the inside corner of the 'L' a mark was made to indicate the location of the first pole. Then six inches along the edge, a second mark was made to indicate the second pole. Then this shape was aligned with the grid on the cutting mat and taped down to the table along one edge. This allowed for the plastic to be moved out of the way and then moved back onto the work space in order to determine the location of each pole as necessary.

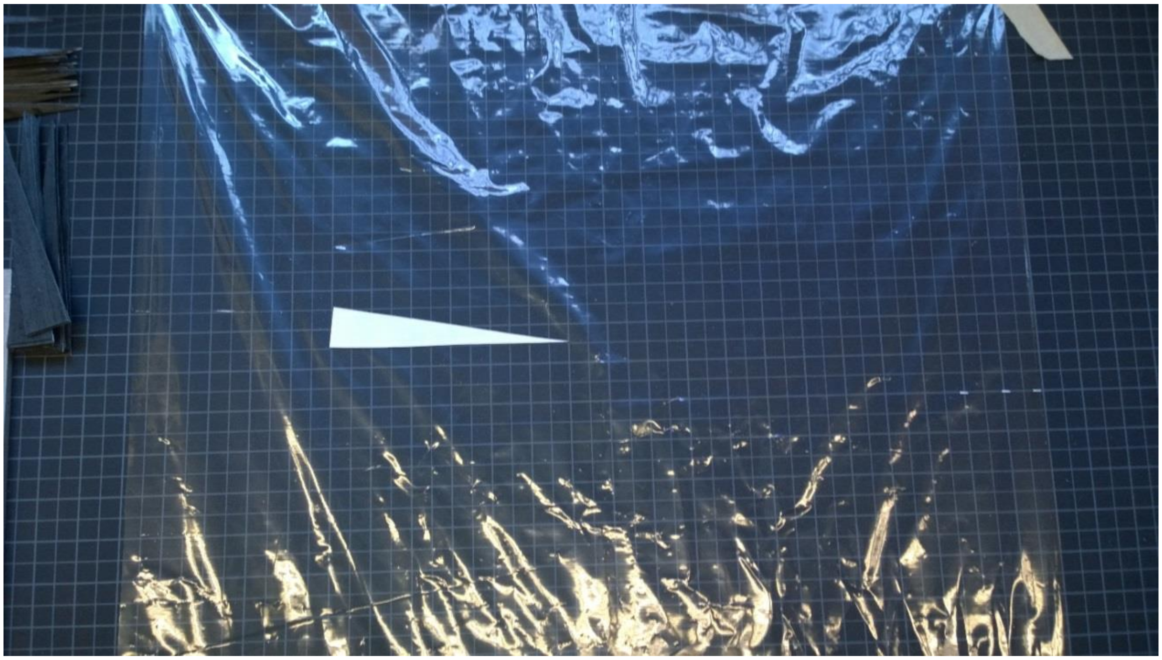

FIGURE 3: PRECISION TABLE FOR TWO-POLE PANEL LAY-UP

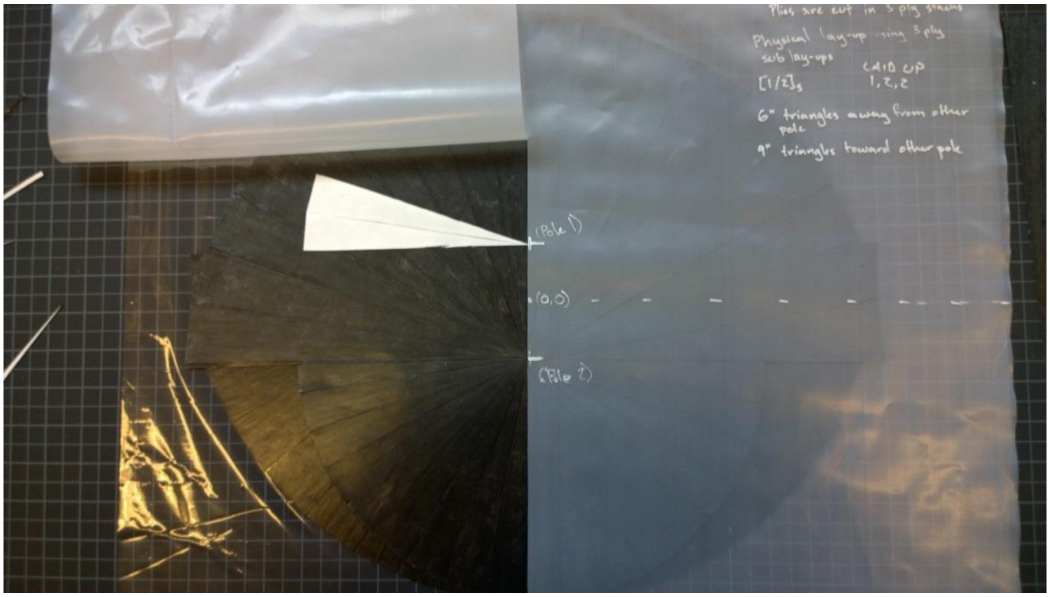

FIGURE 4: L-SHAPE PLASTIC USED FOR LAY-UP

Once the workspace was set up, the triangles were placed by hand in the same circular pattern as the previous panel, however after the first set of 36 triangles (each triangle being a stack of three triangles) were placed, the second and third sets were placed with the tips at the location of the second pole as defined by the plastic ‘L’ shape. The fourth set of triangles were placed with the tips at the location of the first pole. After placing all of the triangles, the whole lay-up was again transferred to a caul plate and vacuum bagged. However, this panel was then cured in an autoclave according to the autoclave cure cycle according to the epoxy data sheet. This panel also warped, however the shape of the panel was determined by the pole location and number of poles. Figure 5 shows the cured shape of the first two pole panel.

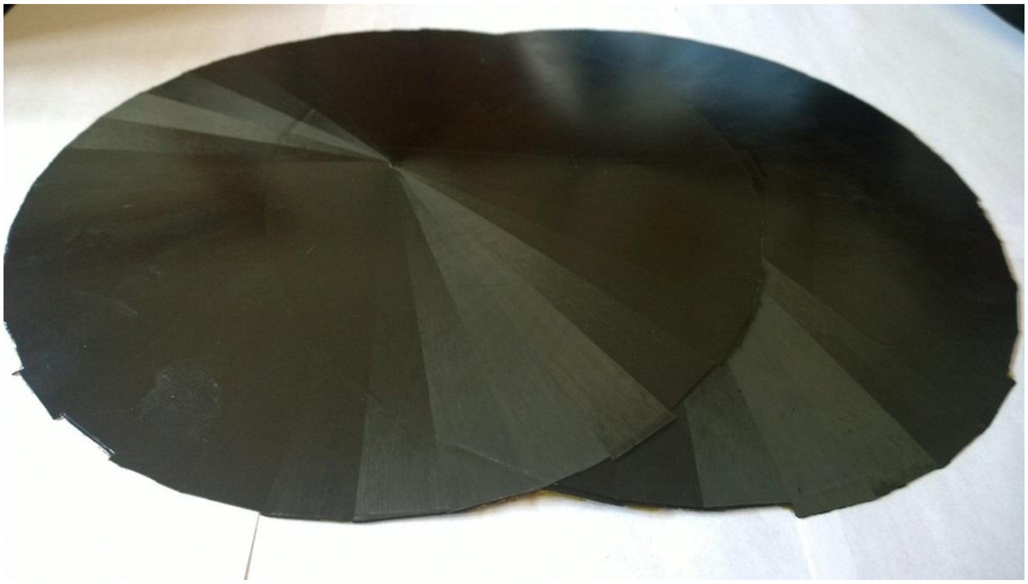

**FIGURE 5: CURED SHAPE OF TWO-POLE PANEL**

The final panel constructed used the same stacking sequence as the second panel, $[(0,3)_3/(0,-3)_3]_s$. The method used for constructing this panel differed in that it was constructed using the above method, but half of the triangles were nine inches instead of six (with wider bases, they also were 10° triangles). This was done so that the final panel to be cut out would result in a twelve inch by six panel. Additionally, before curing the panel, it was cut into a twelve inch by six inch rectangle. It was then placed on a caul plate, vacuum bagged, and cured in an autoclave. After cure, this panel was removed from the autoclave and it also buckled. Figure 6 shows the buckled shape. After this panel, it was determined that any panel constructed with a polar stacking sequence as described above would buckle.

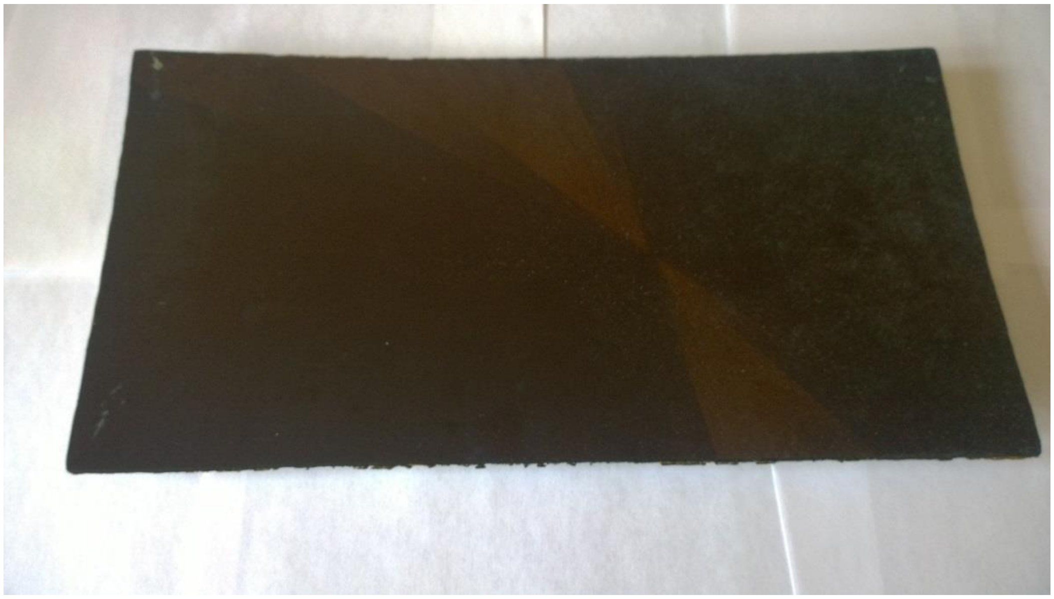

FIGURE 6: CURED SHAPE OF TWO-POLE RECTANGULAR PANEL

After constructing the two pole, rectangular panel, a coordinate-measuring machine (CMM) was used to determine how flat or not flat the panel was and to determine the post-cure dimensions. The CMM used was a Brown & Sharp, Model Gage 2000 with manually controlled probe that was on air brakes. First, the panel was taped onto the measuring surface using blue painters tape. Then three distinct methods were used for measuring and 100 data points were taken for each. The first measurements taken were of the 100 data points laid out in a grid, the second pattern was a spiral, and the third was randomly chosen points. All three sets of data were then entered into a Matlab code (see Appendix A for code) and a 3D surface was created from the data points, the data points can be seen in Figures 7, 8, and 9. Figures 10-12 show the 3D surfaces created from the collected data. The average maximum z-value of the cured shape in the two pole, rectangular panel is about 0.622 inches. This is measured relative to the corners of the panel’s top surface, as set up when calibrating the CMM.

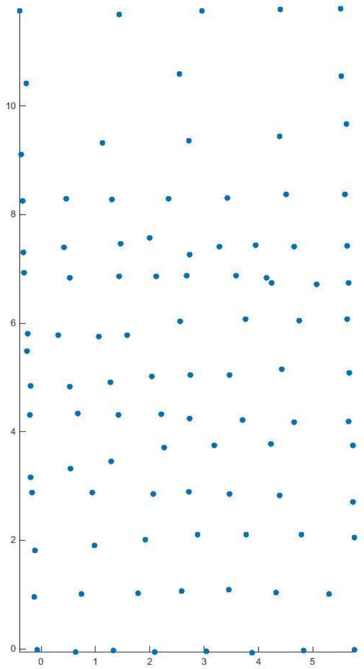

FIGURE 7: CMM POINTS COLLECTED IN A GRID

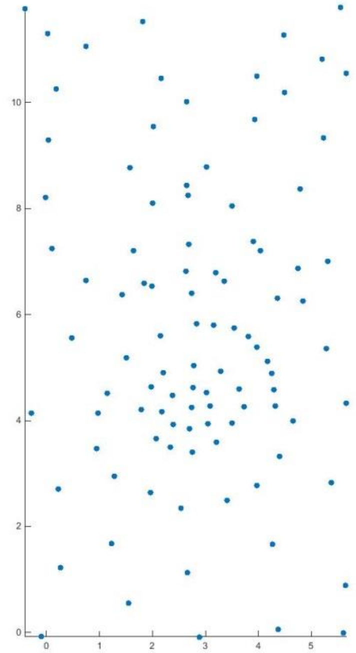

FIGURE 8: CMM POINTS COLLECTED IN A SPIRAL

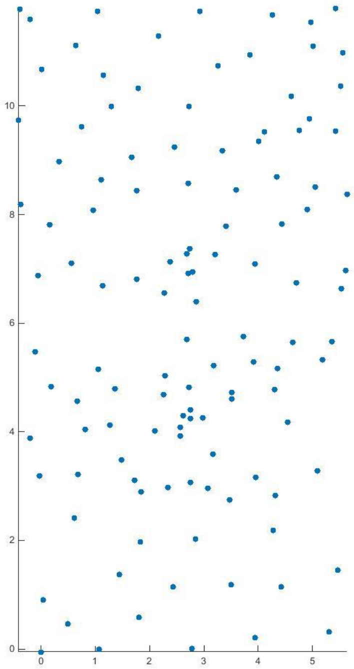

FIGURE 9: CMM POINTS CAPTURED RANDOMLY

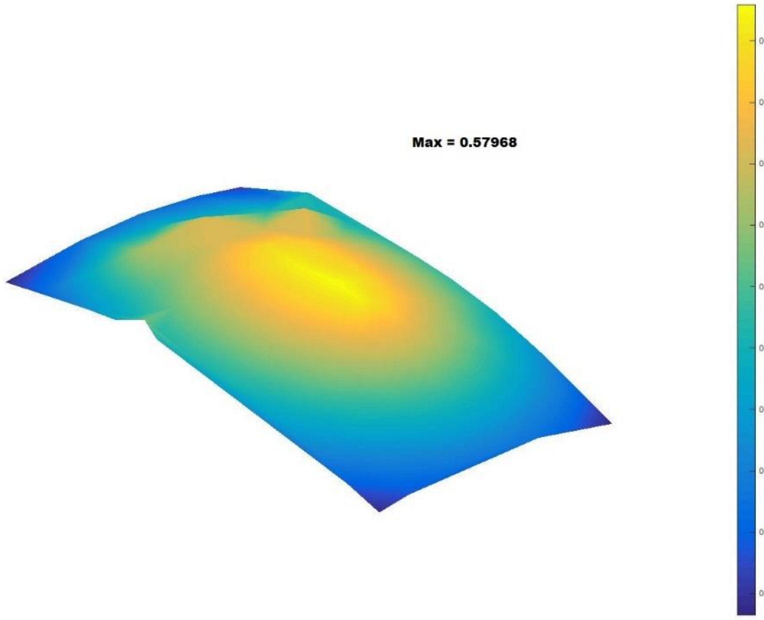

FIGURE 10: 3D PLOT OF GRID DATA

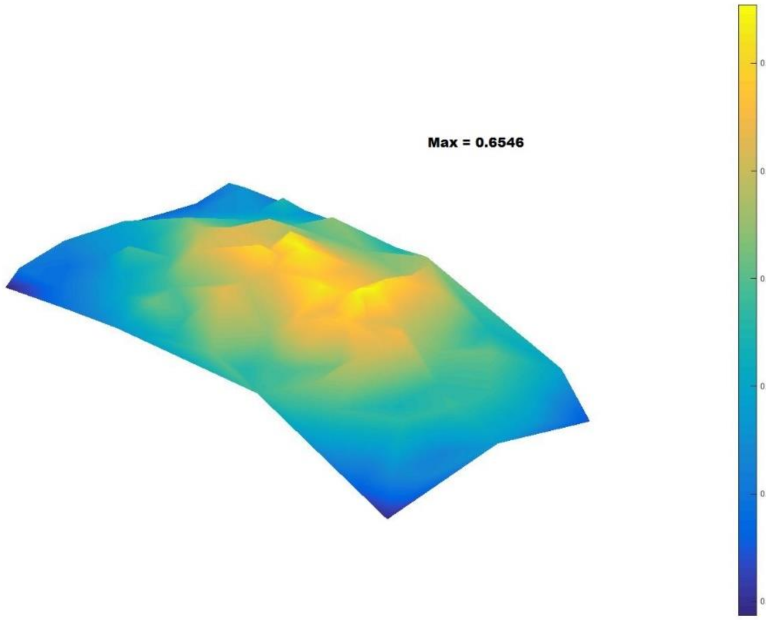

FIGURE 11: 3D PLOT OF SPIRAL DATA

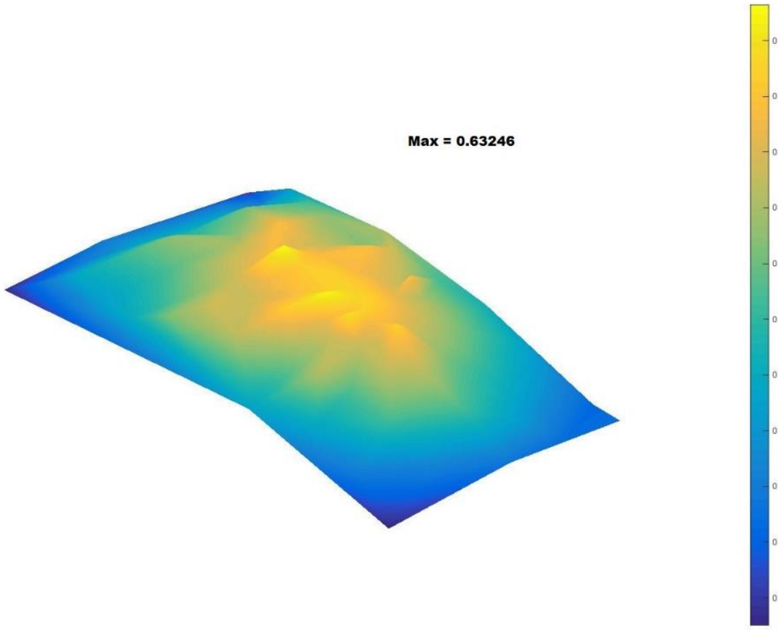

FIGURE 12: 3D PLOT OF RANDOM DATA

## Finite Element Analyses (FEA)

All analyses were performed using the ANSYS Finite Element package along with the ACP (ANSYS Composite Prep/Post) module. Finite element models were created in order to predict the behavior of panels after cure. The ACP package can be used to select a point as the origin for a local fiber coordinate system and then allow that coordinate system to be set up as Cartesian, radial, spherical, or several other options. The radial coordinate system was used for these analyses. When set up properly, the radial coordinates serve as the originating point for all of the fibers, which created the poles in each of the panels.

In order to confirm the validity of the models, several analyses were completed first with simple 0, 90, and cross-ply panels and compared to standard calculations based on classical lamination theory (CLT). The lay-ups for each panel were $[0]_8$, $[90]_8$, and $[45_2/-45_2]_s$. The basic panels were created using the standard Shell 181 element (the default element used by ACP) and the final mesh used is shown in Figure 13. A convergence study was also conducted in order to determine the mesh density needed for a satisfactory comparison to CLT. The boundary conditions were set according to the definitions of a simply supported plate with type S4 supports [20]. FEA analyses based on a 100 lb/in vertical load (parallel to y-axis) applied to the top edge were performed. A comparison of FEA predictions and CLT calculations are presented in the below in Table 1. The mesh for all of the rectangular panels created in this study was the same, unless otherwise noted. The settings used were a mapped face mesh with maximum element size set to 0.05 inches and minimum element size set to 0.01 inches.

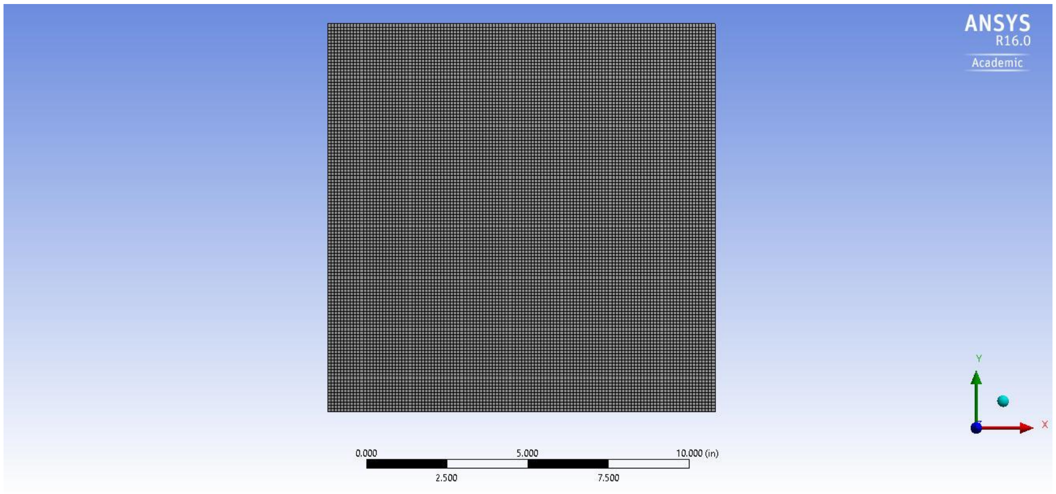

FIGURE 13: FINAL MESH USED TO COMPARE TO CLT

Once the basic analyses were completed and found to agree with the expected results from CLT, the polar coordinate panel models were created. In order to output a comparable answer to CLT and the simple panels, the poles were offset by 10,000 inches from the panel. One pole was placed at (0,10000) and the other at (10000,0). This resulted in the fiber angles from horizontal and vertical being almost 0 degrees, simulating the 0, 90, and cross-ply panels. The same stacking sequences as above were used with these simulated unidirectional and cross-ply panels. Again, the default Shell 181 elements were used and the boundary conditions and loads described above were used. The mesh used was identical to the mesh used previously and can be seen above in Figure 13 and a close up image of both meshes (simulated and non) can be seen including arrows indicating fiber direction can be seen in Figure 14. The results from these calculations are shown in Table 2. Both CLT and the basic panel ANSYS analysis resulted in 46 microstrain in the fiber direction and -15 microstrain in the transverse direction. The offset-pole analysis resulted in 46.04 microstrain in the fiber direction and -14.6 microstrain in the transverse direction.

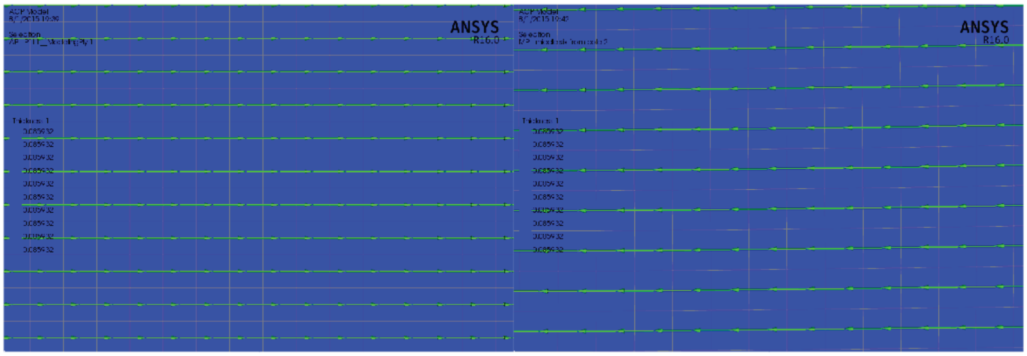

FIGURE 14: SHOWS THE FIBER ORIENTATION OF THE REGULAR PANEL (LEFT) AND OFFSET POLE PANEL (RIGHT)

Once the models were properly set up and the polar coordinate systems were understood, one- and two-pole panel models were created. The one-pole panel model was created with the pole at (0,0) in the center of the panel. The two-pole model had poles at (0,3) and (0,-3). Each model was created using the same Shell 181 elements and the ACP module for stacking sequences. For the one pole panel, the laminate was twelve plies thick with the pole located at (0,0) which was the center of the plate (stacking sequence written as [(0,0)]12). The two pole panel stacking sequence was modeled as $[(0,3)_3/(0,-3)_3]_s$. The first pole location (0,3) was on the outside of the panel and laid up first. The 6 plies with fibers emanating from the second pole (0,-3) were in the middle of the panel. This panel was also twelve plies thick.

The one-pole panel was created using Shell 181 elements as mentioned above from the default settings in ACP. Additionally, after comparing the analysis to the real panel constructed and cured, the layered Solid 185 element was applied to the same model and ran a second time to determine if through thickness effects were causing the differences between the model and the real panel. The Solid 185 element is applied to same ACP stacking sequence after initially setting up the analysis in Workbench and it creates a brick element for each ply through the thickness. In the results section, the comparison and outcomes of these tests will be shown. This panel was created using a twelve inch diameter circle for the geometry. This is also how the physical panel was constructed, so this was the most direct comparison to the constructed panel. The boundary conditions used for this analysis were a displacement set at the center of the circle (on the back surface to simulate the panel resting on a caul plate during cure) and the load was a thermal condition. The environment temperature was set to 355° F and the thermal condition was set to cool from 355° F to 77° F.

The two pole panel was also created using Shell 181 elements and re-run as Solid 185 to check for through thickness effects. However the geometry was different from that of the one pole panel. The two pole panel model was constructed and cured in two different geometries, so two different models were created. The first model was created with two overlapping twelve inch diameter circles, the same as the first physical panel was constructed. The second model was created as a twelve inch by six inch rectangle, the same as the second physical panel constructed. The thermal condition described above was applied to both of these panels.

For the first two pole panel, the boundary condition was set as a displacement along the back edge of the panel with displacement in the z-direction set to 0 inches. Ultimately this analysis was discarded because the second two pole panel model was more appropriate and the boundary conditions were closer to those applied to the physical panel. The boundary conditions used on the second two pole panel were four displacements, one applied at each of the four corners of the panel on the back. The lower right corner had zero displacement in x-, y-, and z-directions. The upper right corner had zero displacement in x- and z-directions, free in the y-direction. The lower left corner had zero displacement in the y- and z- directions, free in the x-direction. The upper left corner had zero displacement in the z-direction and was free in the x- and y-directions.

Many different combinations of boundary conditions were examined and ultimately discarded as incorrect methods of modeling the cure process for the flat panels. The initial intent of these three models was to create a flat panel and then apply tensile and/or compressive loads to the model in order to determine laminate properties and develop a better understanding of the mechanics involved in the construction of the hemispherical dome. However, as will be discussed in the results section, it was ultimately determined that creating flat panels with this polar methodology was impossible. Therefore, the further application of tensile and/or compressive loads was unnecessary and the models were repurposed to study the curing of the panels and trying to understand and simulate the mechanics of curing panels constructed with this polar methodology.

It was also of interest to determine the effect of the discontinuity in the fibers at the pole locations. In the physical panels, the fibers radiate outward at the poles, which leaves a discontinuity at the pole and therefore the panel is mostly resin at that point in each ply, ignoring overlap of the fibers. In the finite element model, the default state of the panel is that the fibers at each pole are not discontinuous. In order to determine the differences between modeling the discontinuities and leaving the fibers continuous at the poles, the two pole panel with rectangular geometry was chosen as the test subject because it was the easiest to compare to the physical panel. The model was first run with the fibers continuous across the poles and then run again with empty holes in the panel at the pole location. The holes were diameter 0.01 inches across and no material was applied to them. The panel was run a third time with epoxy only material properties applied to the resin rich zones. The results of these analyses are discussed below in the results section and shown in Table 6 in the results section. Convergence study with mesh left off because the model was the same as previous models that already had a convergence study done.

Once the linear analyses were run, the next step in trying to simulate the cure process of these polar panels was to construct models that capture thermal buckling effects due to curing the panel and the mismatch of coefficients of thermal expansion between the epoxy and the fibers. Again, the two pole panel model was selected for modeling these problems because of simplicity in comparisons. Both eigenvalue buckling simulations and non-linear buckling simulations were run and again a variety of boundary conditions were tested. As above, the boundary conditions used for the two pole panel ultimately were selected as the best match to real curing conditions. This meant that a displacement condition was applied to each corner with displacement in the z-direction held at 0 inches in all four corners. In the lower right corner, displacement in the x- and y-directions were also held to 0 inches; in the upper right corner, displacement in the x-direction was also held to 0 inches; in the lower left corner, displacement in the y-direction was also held to 0 inches; finally, in the upper left corner, no other displacements were set. The loading condition for these buckling analyses was different for the eigenvalue buckling analysis and the nonlinear problem.

To apply an eigenvalue buckling analysis to the panel, first a linear static structural analysis must be run. Once the static structural analysis is set up, an eigenvalue buckling analysis may be attached to the static structural analysis in ANSYS Workbench. The settings from the static structural analysis, including boundary conditions and loads, are shared with the eigenvalue analysis and by default are used to compute the load factor, $\lambda$. ANSYS, by default, would output the first two load factors, positive or negative. A setting can be turned on to only allow positive load factors and the number of load factors found can be increased from two. In the situation described for this research, it was often necessary to turn on only positive load factors or increase the number of load factors found as the first set was often negative indicating the panel would buckle if it was heated rather than cooled.

For the eigenvalue buckling analysis, several thermal conditions (set in the static structural analysis) were used in order to confirm the output load factor. The input for the thermal condition was the environment temperature of 355° F and a target temperature it was cooled to. The output was the load factor lambda (λ). The environment temperature was held constant and the final, cooled temperature was varied, the input temperatures are shown in Table 3.

**Table 1:** Shows the input temperatures and resulting load factor for the eigenvalue analyses run.

| $T_{input}$ ($T_{ref}$ = 355° F) | $\Delta T$ (°F) | Load Factor, λ | $T_{Buckle}$ (°F) |
|---|---|---|---|
| 150 | -205 | 0.737 | 228.09 |
| 100 | -255 | 0.592 | 227.97 |
| 77 | -278 | 0.543 | 227.95 |

The nonlinear analyses was set up exactly the same way as the above two pole panel with rectangular geometry (also the same as the eigenvalue problem), but instead of applying an eigenvalue analysis, large deflections were turned on in Workbench, which signals the program to run a non-linear analysis. The default auto time stepping controls were used and the solution converged successfully.

In order to determine whether or not ANSYS can accurately predict the behavior of panels with non-symmetric stacking sequences, several analyses were performed to compare to the near-closed form solution developed by Hyer for non-symmetric $[0_x/90_x]_T$ panels [14]. Specifically a $[0_4/90_4]_T$ panel was considered. To do these analyses, a square panel was created and the material properties provided in Table 2. The boundary conditions used were the same as described above for the rectangular two-pole panel (displacement BCs in the four corners, allowing the panel to contract but not move or rotate). The same thermal load condition was applied as a cooling load from 350 degrees to 77 degrees F. In order to compare the results to the solution published in [13] analyses were run with the edge lengths of the square panel in increments of 30 mm from 30 mm to 3000 mm and the radius and radius of curvature were calculated using Equations 1 and 2. Figure 15 shows the geometry and variables involved in this equation. K is the radius of curvature.

$$R = (\frac{c^2}{4h} + h)/2 \tag{1}$$

$$\kappa = \frac{1}{R} \tag{2}$$

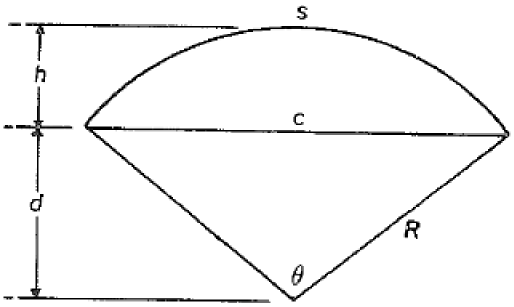

**FIGURE 15: GEOMETRY USED FOR EQUATION 1**

The Hyer solution predicts a saddle shape at low edge lengths (i.e. thicker panels) and an almost right cylinder for thin panels. The analyses performed using ANSYS ACP resulted in a saddle shape for all edge lengths (both thin and thick panels). An image of the ANSYS result is shown in Figure 16. Table 17 in Appendix E shows the z-deflection results and curvatures of the analyses run at different panel lengths. Figure 65 in Appendix E shows the plot of curvatures versus edge length. It can be seen that the curvature is decreasing slightly, however when compared to the plot shown in [13], it is clear that the effect of warping due to unsymmetric stacking sequence was not captured by these analyses.

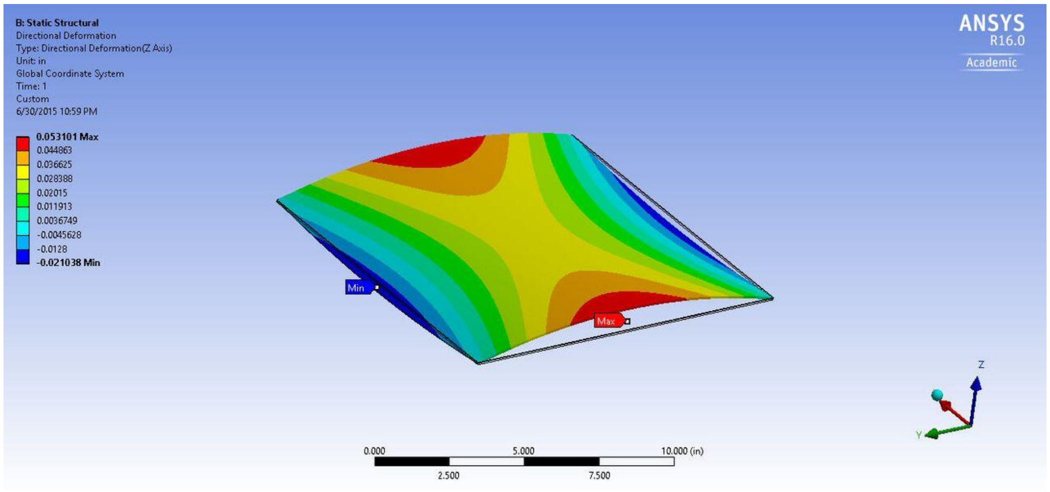

**FIGURE 16: HYER ANALYSIS RESULT**

At the time of writing this report, it has not been determined whether or not ANSYS can accurately capture the effects of cooling on a composite panel with an unsymmetric stacking sequence. The research reported on here constructs a framework for analyzing structures created using a polar stacking sequence, however further research needs to be done to validate the models and the ability of ANSYS to capture the effects of the unsymmetric and polar lay-ups. Research done by Hyer in [8] indicates that these analyses can be done with the ABAQUS finite element package. Due to this, it is unlikely that ANSYS is incapable of performing these analyses, and rather it is likely that the reason ANSYS has not matched the Hyer solution at the time of this writing is human error in setting up the boundary conditions. Hyer suggests fixing a central node and allowing the shape to deform at all edges and corners. More work is necessary in order to validate the models presented here and in Hyer's work [8] and many other papers published by Hyer and his group, the difficulties associated with capturing this phenomenon are discussed.

## Digital Image Correlation

After measuring the deformed shape due to cure, the two pole panel was prepared for DIC in order to confirm the measurements and to prepare for performing DIC on the dome. One of the major difficulties with DIC was getting the proper speckle resolution on a large surface and the panel was sufficiently large to practice speckling at the correct resolution. The first step of preparing for DIC was to spray the panel matte white so that the black speckles would contrast significantly. Then the panel was speckled with matte black spray paint through a fine mesh frame. The mesh collected the largest drops of paint and the paint was sprayed above the panel such that the finest particles missed the panel while the heavier (larger) drops fell onto the panel. The panel was also orientated at a slight angle off from vertical. The spray paint used was VHT branded, which had a different nozzle from most other brands and the paint could be used for very high temperatures. The nozzle is pictured below in Figure 17.

**FIGURE 17: SPRAY NOZZLE FOR DIC SPECKLES**

After speckling the panel, the DIC system was set up to take a preliminary image to determine the shape of the panel in the z-direction and to test the resolution of the speckling on the images. The DIC system used consisted of two digital cameras, mounted on a tripod with multiple angle adjustments and a linear track for sliding the cameras side to side. Figure 18 shows the DIC system. The system was connected to a computer running VIC 3D DIC software from Correlated Solutions. Once the system was set up, the cameras had to be focused onto the panel, with centers approximately stacked, in order to effectively capture the 3D images necessary to do strain analysis.

After the cured shape of the panel was captured using DIC, the panel was tested in order to capture the buckling behavior. In order to capture these effects, the panel was heated to its cure temperature of 355° F in an oven and held this temperature for two hours. The panel was removed from the oven and quickly taped to the wall in the same location with the same set up for the DIC system as the previous images which allowed for immediate image capture. The VIC Snap software was set to capture three images per second for five minutes in order to observe deformations that developed during the cooling process.

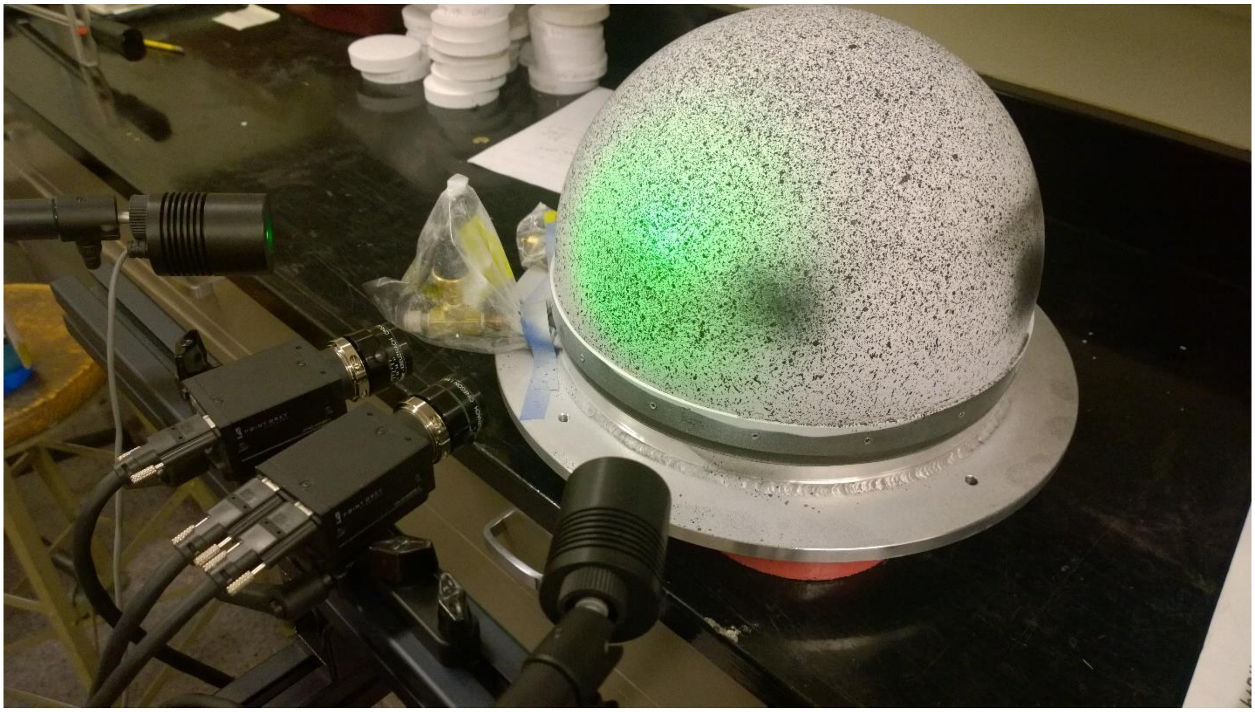

**FIGURE 18: DIC SETUP FOR DOME**

Additionally, the first panel constructed with a one pole, twelve ply stacking sequence was heated to 355° F and held for two hours. After heating, the panel was removed from the oven and then 'popped' through to check for buckling. Since the buckled shape would be stable in either direction, popping the peak through to the other side would confirm that there were two stable buckled shapes, however doing so without heating it first could have destroyed the panel since it was constructed from triangles and mostly held together with epoxy between the panels. Figure 18 shows the deformed shape of the one-pole panel.

FIGURE 19: SHAPE OF ONE-POLE PANEL

## Analysis of Dome

### Geometry and Production

The dome studied was made up of a fourteen inch diameter hemisphere with a three inch cylindrical collar around the base. The collar was added in order to safely clamp and pressurize the dome. The process of constructing the dome involved the following steps [19]:

1. Produce a male foam plug
    a. Adhesively bond three foam blocks
    b. Mill to spherical shape
    c. Sand/prime/wax surface
2. Produce female composite tool
    a. Layup
    b. Vacuum bag
    c. Cure
3. Produce composite dome
    a. Prepreg “peels” cut from unidirectional tape
    b. Hand-layup of peels in composite tool
    c. Vacuum bag

The dome was built with an eight ply thick stacking sequence using “peels” (analogous to the flat plate triangles). The peel dimensions were such that the doubly-curved surface of a hemisphere could be completely covered.

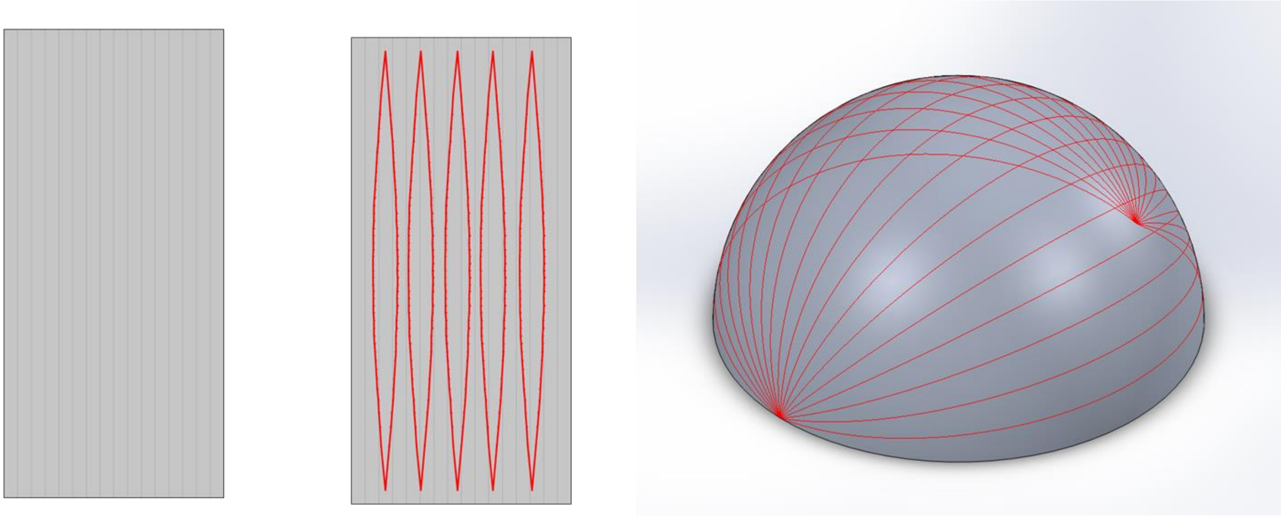

FIGURE 20: PEELS FOR DOME CONSTRUCTION

In order to describe the plies and stacking sequence, as with the flat plate, the poles were specified, however with the dome, latitude and longitudes of each ply pole were used. In Figure 20, the poles are shown are on the equator at 0° latitude and the “prime meridian” was defined as the arc passing through the poles on the equator, therefore the pole location for this ply, and thus the label for this ply, is (0°/0°). The ply containing the top most, or “north pole”, has all meridians passing through it and was designated as (90°/θ). The final stacking sequence of the dome is given as: [(0°,0°)/(45°,45°)/(90°, θ)/(45°,-135°)/(45°,135°)/(90°, θ)/(45°,-45°)/(0°,0°)].

The dome was produced using six unique pole positions, as seen above, that varied from ply to ply and due to this variation, the stacking sequence varies from point to point and an algorithm similar to that of the flat panels has been developed to calculate the fiber angle in each ply at any point on the dome.

Prior to the author’s involvement in this project, a code was developed in Fortran to determine the fiber angle at any given point on the surface of the dome when the number of poles and pole locations were specified. The calculations used a similar approach as used for latitude and longitude calculations on a globe.

## FEA

The dome was also modeled using ANSYS Workbench with the ACP module. The geometry used is shown below in Figure 21, the slices show the different paths used to output the strains off the surface of the dome. As with the physical dome, it consisted of a fourteen inch diameter hemisphere with a three inch collar at the base. It was constructed as a revolved surface with no thickness and the thickness was applied later in the process when the stacking sequence was defined. Just like with the physical construction of the dome, the stacking sequence was directed towards the inside of the dome, resulting in the outer ply being closest to the fourteen inch diameter size.

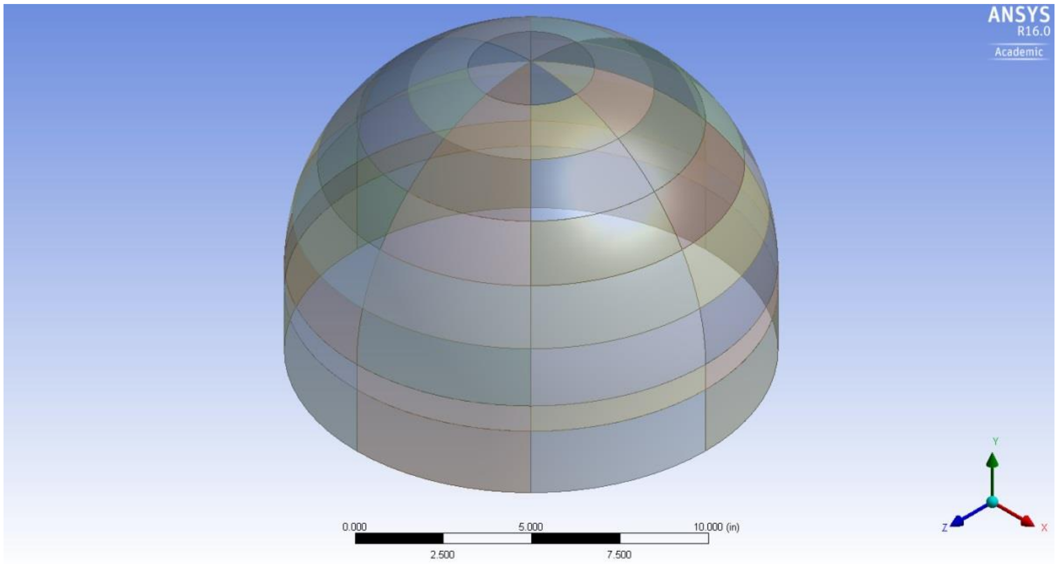

**FIGURE 21: DOME FEA GEOMETRY**

The layered shell 181 element which ACP uses as its default, the same as above for the panels, was used for the dome analysis. The mesh was set up in a variety of ways and the final mesh used was split into many smaller regions (slices) in order to better fit the mesh onto the surface and to provide avenues for the outputs required to compare directly to strain gauge measurements. The final mesh can be seen in Figure 22. There were 21415 nodes and 24324 elements.

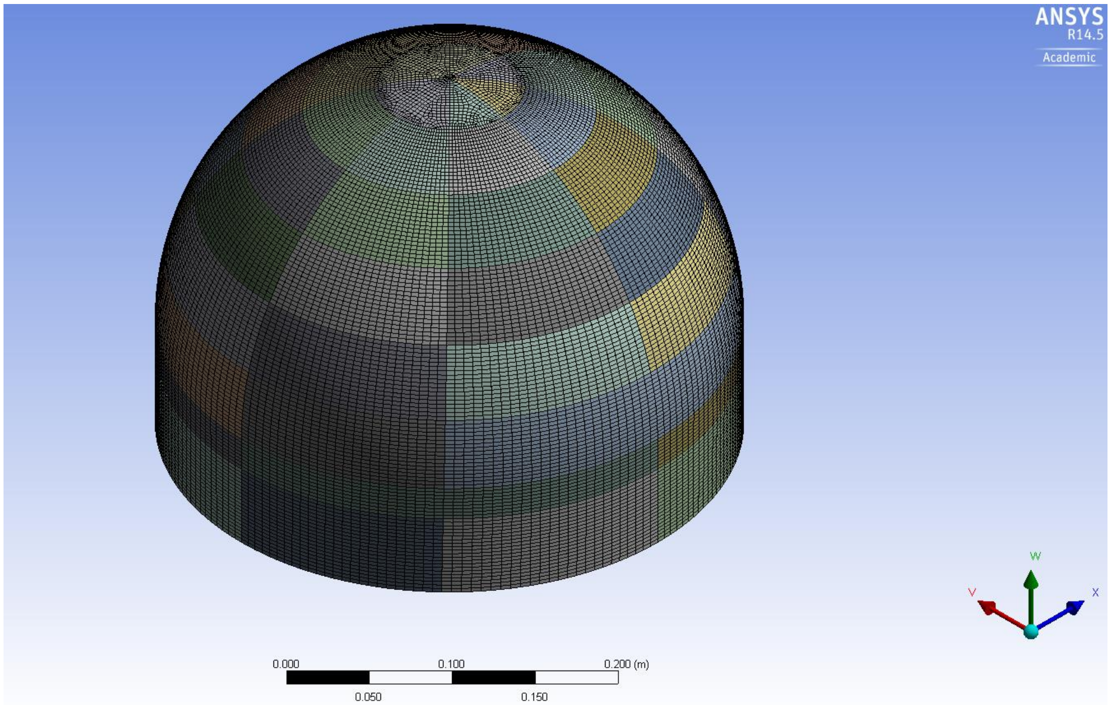

FIGURE 22: DOME MESH

In the ACP settings, the plies were applied to the dome surface with the stacking sequence discussed in the previous section, [(0°,0°)/(45°,45°)/(90°, θ)/(45°,-135°)/(45°,135°)/(90°, θ)/(45°,-45°)/(0°,0°)]. Figure 23 shows the fiber orientation in the (90°, θ) ply and Figure 24 shows all six pole positions used in the model. Here the thickness of the plies was set, along with the radial rosettes, and the stacking sequence for the collar (chosen to be quasi-isotropic due to complications arising from the polar nature of the structure. Each pole location required a rosette to be created at the pole location on the surface and set to be radial coordinates, allowing the fibers to radiate outward from the pole. It was of note that these fiber directions were truly radial, which was slight different from the peels created during construction of the dome. For the collar, the peels created problems in defining the fiber angles because the fibers were still radiating outward from the poles and there was no way to attach the collar to the dome if the excess fibers from the poles were cut off. Therefore it was assumed that quasi-isotropic, 8-ply properties for the collar would be sufficient.

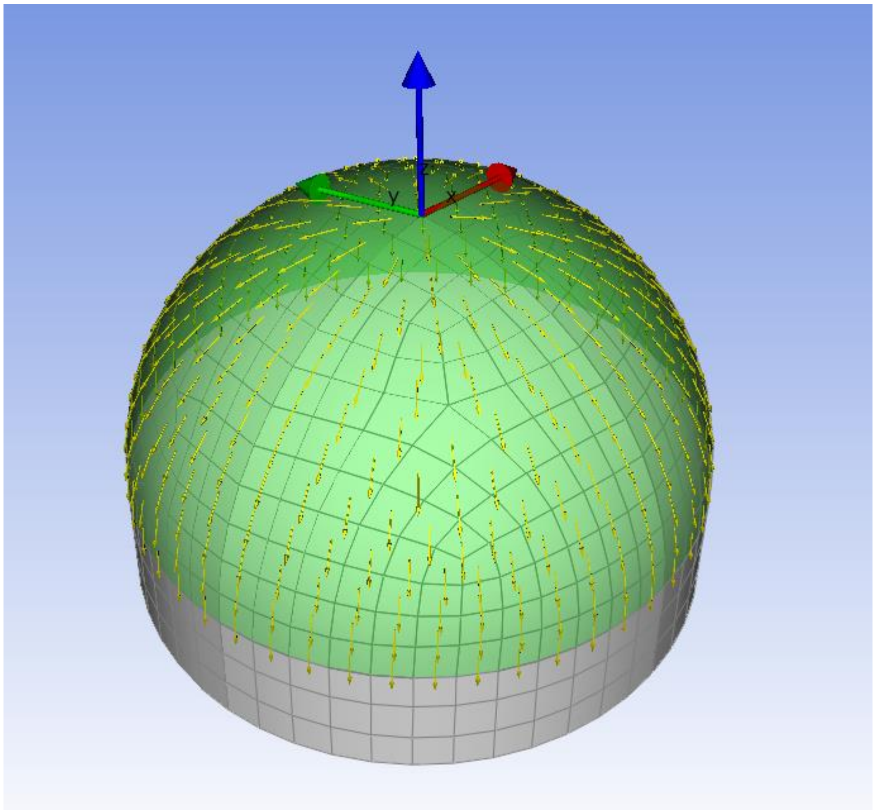

FIGURE 23: DOME FIBER ORIENTATION FOR (90,Θ) PLY

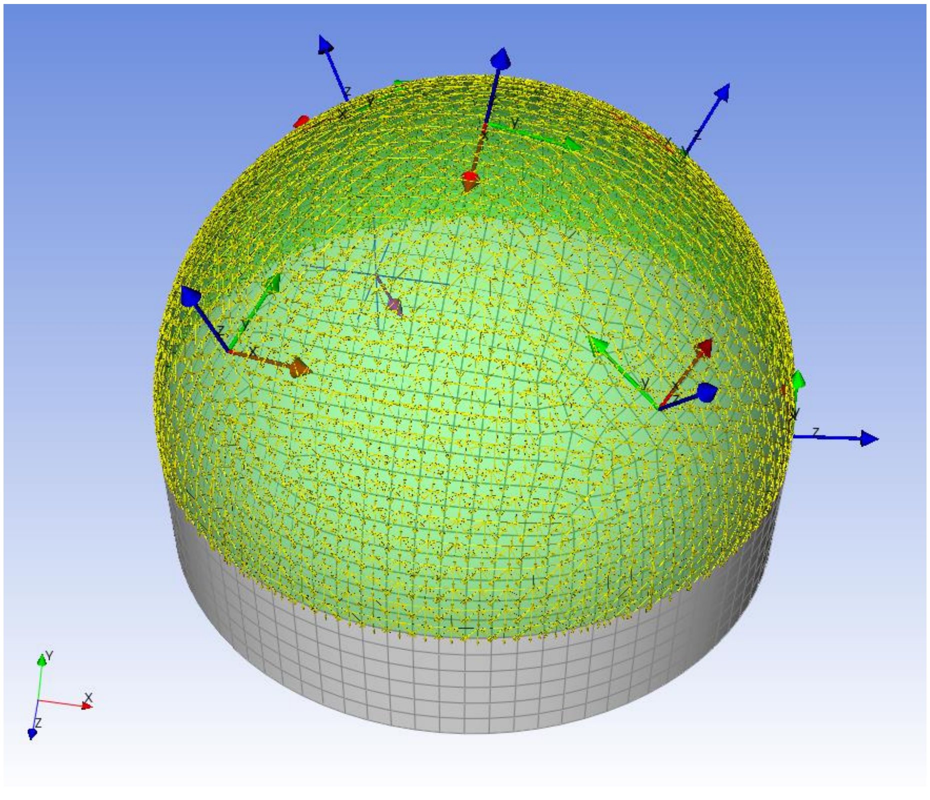

FIGURE 24: FIBER ORIENTATION FOR ALL PLIES

Once the geometry was set up, meshed, and the stacking sequence was applied, the first test applied was a thermal test to determine whether or not the dome buckled during cure. Similar to the panels above, a thermal condition was applied with a reference temperature of 355° F and the dome was cooled to room temperature or 77° F, a change in temperature of -278° F. A standard linear analysis was run first, followed by an eigenvalue buckling analysis, and finally a non-linear analysis to confirm the expected results. All three analyses used the same boundary conditions. Since the dome was cured <this way>, the boundary conditions were set as <this way>. For the linear analysis, no other inputs were required. For the eigenvalue buckling analysis, the static structural (linear) analysis had to be run and then the eigenvalue buckling analysis attached to the backside of the static structural analysis, but there were no other differences in setting up. Finally, on the non-linear analysis, the large deflection setting was changed to 'On' and the auto time stepping settings were left to the program to decide.

## Measurements

It was necessary to measure the strain on the surface of the dome in order to compare to the numerical solution from ANSYS. In order to do this, three different methods were used including resistance strain gauges, fiber optic strain gauges, and Digital Image Correlation (DIC). For all three of these methods, an aluminum fixture was developed for the dome to clamp onto. The fixture can be seen in Figure 25.

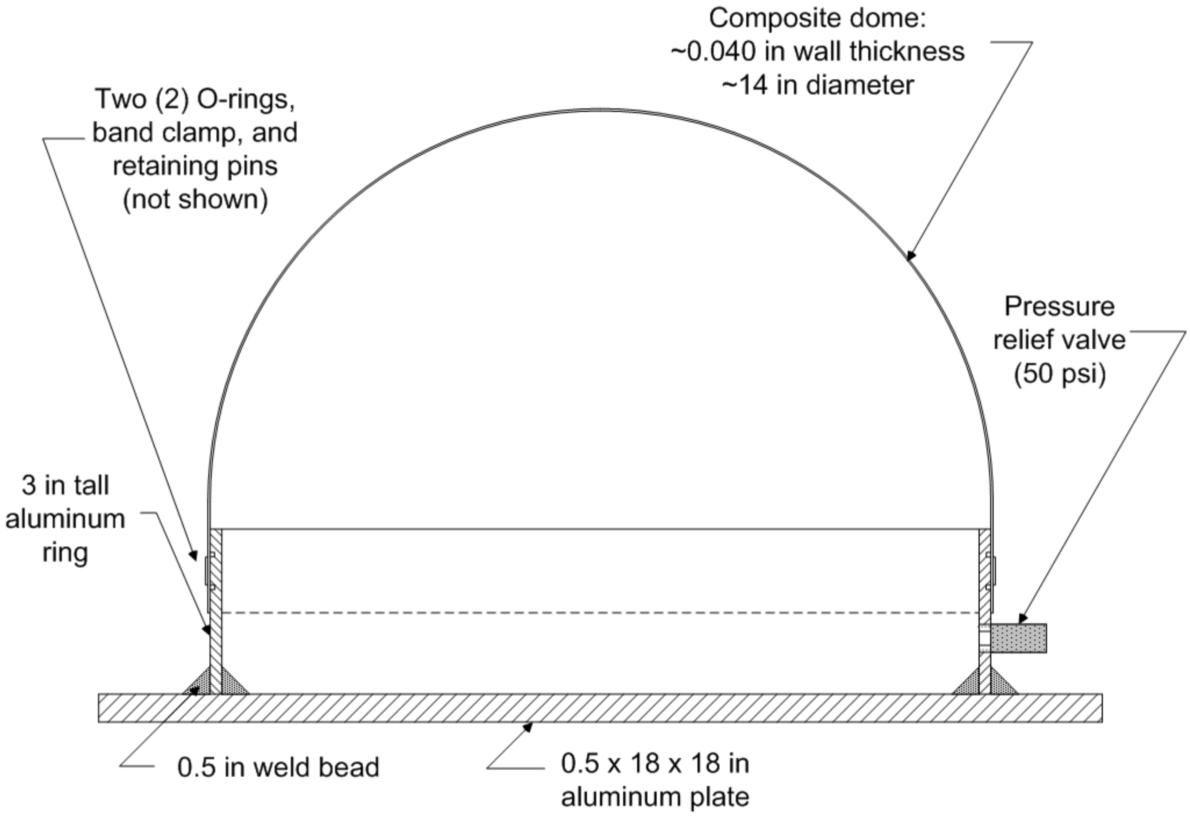

FIGURE 25: DOME TEST FIXTURE

It consisted of a half inch thick aluminum plate as the base, with a fourteen inch diameter cylinder with quarter inch wall thickness welded onto the plate. Then two holes were drilled and tapped through the cylinder wall for the pressure relief valve and pressure inlet plus a pressure gage. In order to create a good seal between the dome and the aluminum cylinder, the top two and a half inches of the cylinder were turned on a lathe to achieve a smooth surface finish and the inside surface of the composite dome was sanded smooth by hand. Additionally, two o-ring seats were added to the aluminum cylinder in order to seal the dome on the inside. Next, the dome was slid onto the cylinder and firmly pressed into place for positioning. Once the dome was in place, a thin piece of rubber was slid between an eighth inch thick steel band clamp and the dome and the clamp was cinched into place. The final step was to drill holes through the band clamp and the dome and partially through the aluminum cylinder being careful not to pierce the inner wall. Two of these fixtures were made, one for the strain gauge dome and one for the dome DIC was performed on.

Once the first fixture and dome were assembled, three element rectangular stacked rosettes were bonded along the 0° and -90° meridians, as seen below in Figure 25. A total of 13 rosettes were used which resulted in a total of 39 strain gauge elements. The gauges used were M-M C2A-06-125WW-350 standard resistance strain gauges [19]. The system used to output the measured strains was a Vishay System 5000 with 20 channels.

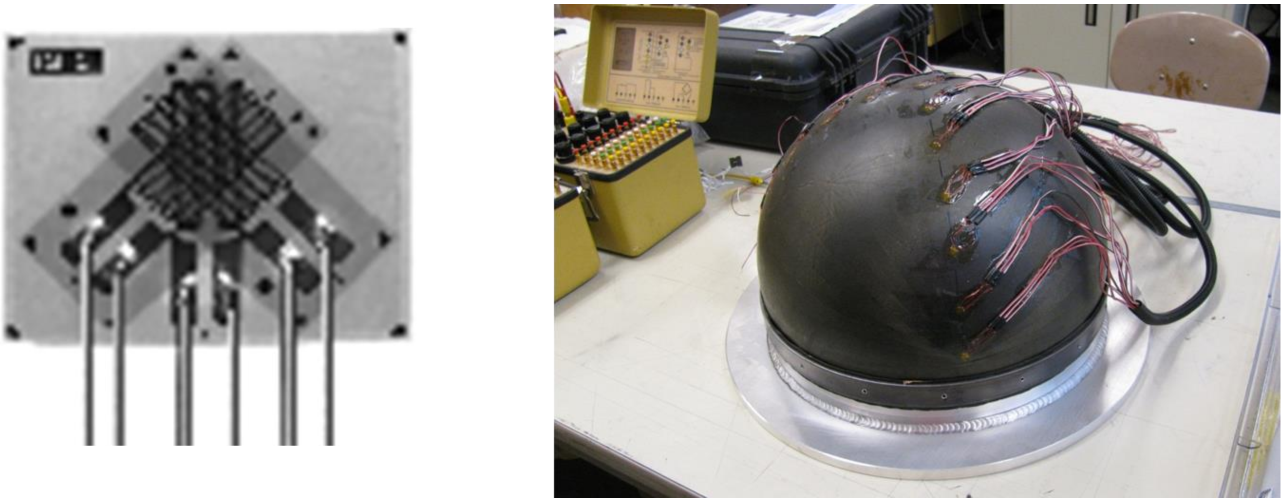

FIGURE 26: STRAIN GAUGE ROSETTE AND DOME WITH STRAIN GAUGES MOUNTED

These rosettes were each oriented so that one strain gauge was parallel to the meridian it laid on, one was at 45 degrees to it, and the third was parallel to the latitudinal lines.

After collecting data with the resistance strain gauges, they were removed from the dome and a 10 meter long optical fiber used to sense strains was bonded to the dome using M Bond 200 strain gage adhesive from Vishay. The strain measurement system used with the optical fiber was Luna Technologies ODiSI-B optical strain sensor. The fiber was bonded to the dome such that hoop strains at the following latitudes could be measured:

- 0°
- 15°
- 30°
- 45°
- 60°
- 75°

Additionally, the fiber was bonded to the dome such that meridional strains could be measured at the following latitudinal positions:

- 0°
- 45°
- 90°
- 135°
- 180°
- 225°

- 270°
- 315°

Figure 27, below, shows the optical fiber bonded to the dome.

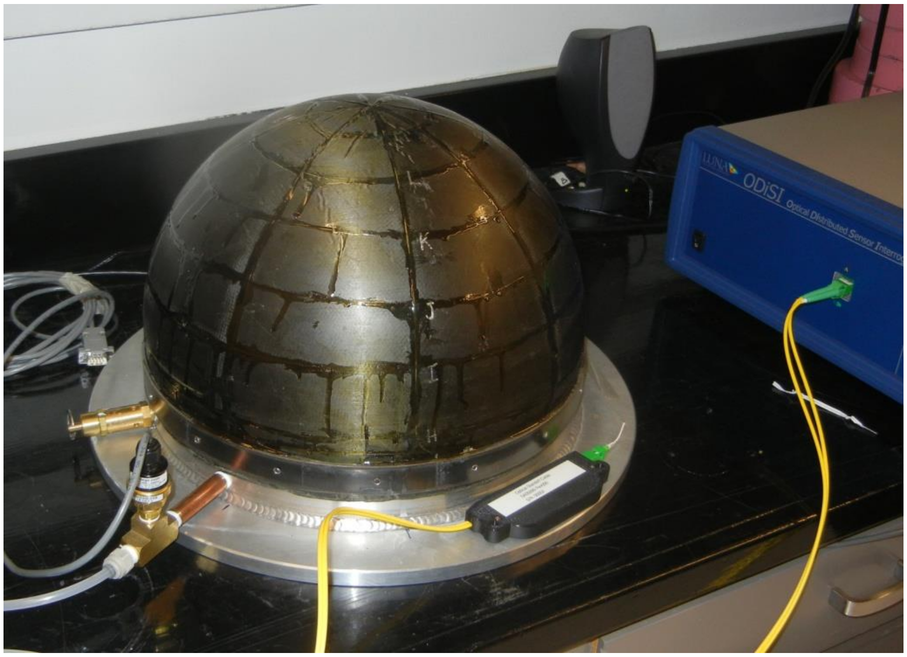

FIGURE 27: DOME WITH FIBER OPTIC CABLE

The second dome was used for DIC, but before preparing for DIC, it was measured using a coordinate-measuring machine (CMM). The CMM used was a Brown & Sharp Model Gage 2000. The dome was measured to determine how close to spherical it was by using the spherical measurement setting in the software. It was measured using 5, 10, 20, and 40 data points in order to confirm the results of the measurement.

After measuring the dome with the CMM, the final measurements to be taken were with DIC. Since DIC requires high contrast speckling patterns on the surfaces of interest, the dome was first spray painted white with standard Rustoleum branded, matte white spray paint. Then it was speckled using Rustoleum branded, matte black spray paint. Rustoleum was chosen because of the design of the spray nozzle, the nozzle was much easier to control the flow of paint through by hand than other brands and was ultimately determined to be better than the VHT brand paint cans used for the panels. For the same reasons as with the panel, the spray can was held above the surface to be speckled and the paint was allowed to fall onto the surface through a mesh. However, when speckling the panels, the face was relatively flat and it was easy to control the speckles falling onto the surface. Since the dome was spherical, the speckles fell onto the surface at different angles and often dripped down the surface. The speckling process required careful control of how much paint came out and how much pressure was applied to the nozzle and even with careful control, paint had to be removed with acetone several times.

After the speckling process, the dome and fixture were hooked up the pressure lines and the DIC system was set up. The DIC system used consisted of two digital cameras, mounted on a tripod with multiple angle adjustments and a linear track for sliding the cameras side to side. The system was connected to a computer running VIC 3D DIC software from Correlated Solutions. Once the system was set up, the cameras had to be focused onto approximately the same area of the dome in order to effectively capture the 3D images necessary to do strain analysis. The dome was broken up into ten regions around the circumference in order to make capturing the images coherent. The only way to fully capture a cylindrical or spherical object with DIC is to set up a system of cameras that completely surrounds the object, usually with 6 to 8 cameras. Since this was not feasible, the two camera system was used and the dome was rotated in place. Afterward, the images were stitched together using Adobe Photoshop and Adobe Illustrator. Vertically, the dome was split into three sections, for the same reasons as above. Images were taken at 0 psi and at 10 psi intervals up to 50 psi and strains in the x- and y-direction were captured as well as principal strains, $\varepsilon_1$, $\varepsilon_2$, and $\gamma_{12}$.

# Results

## Material Properties

The material property tests were conducted in accordance with ASTM D3039 and analyzed accordingly using the output from the Instron Tensile Testing Machine Model 5585H. The Instron was set up to measure load and track the crosshead displacement of the samples. Table 4 below shows the calculated laminate properties. Plots are shown in Appendix C for reference. The strains were output by the resistance strain gauges mounted onto the front and back of the tensile coupons. This resulted in front and back surface measurements that were then averaged and used for calculating the laminate properties.

**Table 3:** Shows laminate properties as determined by ASTM D3039 standards for Toray T800-3900 carbon fiber/epoxy pre-preg.

| | |
|---|---|
| $E_{11}$ (msi) | 25.32 |
| $E_{22}$ (msi) | 1.218 |
| $\gamma_{12}$ | 0.316 |
| $G_{12}$ (msi) | 0.687 |
| $\alpha_{11}$ (°F$^{-1)}$ | $-3.11 \times 10^{-7}$ |
| $\alpha_{22}$ (°F$^{-1}$) | $1.67 \times 10^{-5}$ |
| Ply thickness, t (inches) | 0.007161 |

## Flat Plate

In order to confirm that ANSYS accurately predicts known solutions from CLT, several analyses of simple flat panels were run. These analyses were then compared to known CLT solutions developed from code written by Professor Mark Tuttle called SPORTHO. SPORTHO was written in fortran as a way to analyze specially orthotropic (SPORTHO) laminates using CLT. A thorough description of the code and how to use it can be found in [20].The model used was a rectangular plate with the material properties listed in Table 4 above. The load applied was a thermal load cooling the part from 355° F to 77°F and subject to simple supports of type S4 [20]. Three stacking sequences were used: $[0]_{12}$, $[90]_{12}$, and $[0_3/90_3]_s$. The analysis was run as an eigenvalue problem and the outputs compared were the predicted buckling temperature. A sample of the results found from these analyses can be found in Tables 4 and 5. The rest of the results can be seen in Appendix D.

After comparing several simple panels, the ANSYS analyses were switched to flat panels constructed using simulated fiber angles. To do this, the offset-pole polar stacking sequence methodology described previously was used. Two poles were set at 10000 inches off of the origin at (10000,0) and (0,10000). Since the poles were removed from the panel by a large distance, the fiber angles were approximately 0° and 90° which allowed for comparisons between SPORTHO results, the simple flat panel results, and the simulated simple panel results. These results can be found in detail in Appendix D.

**Table 4**: Shows a sample of the results from the basic CLT analyses and the ANSYS analyses run for comparison to validate the models created.

| Stacking Sequence | a (side length in the x-direction) | b (side length in the y-direction) | $T_{Buckle, SPORTHO}$ (°F) | $T_{Buckle, ANSYS}$ (°F) | % Error |
|---|---|---|---|---|---|
| $[0]_{12}$ | 12 | 12 | 108.5 | 108.17 | 0.3 |
| $[90]_{12}$ | 12 | 12 | 108.5 | 108.17 | 0.3 |
| $[0_3/90_3]_s$ | 12 | 12 | 145.4 | 144.5 | 0.62 |

**Table 5**: Shows a sample of the results from the offset pole CLT analyses and the ANSYS analyses run for comparison to validate the models created.

| Stacking Sequence | a (side length in the x-direction) | b (side length in the y-direction) | $T_{Buckle, SPORTHO}$ (°F) | $T_{Buckle, ANSYS}$ (°F) | % Error |
|---|---|---|---|---|---|
| $[0]_{12}$ | 12 | 12 | 108.5 | 108.11 | 0.36 |
| $[90]_{12}$ | 12 | 12 | 108.5 | 108.11 | 0.36 |
| $[0_3/90_3]_s$ | 12 | 12 | 145.4 | 144.5 | 0.62 |

The first panel constructed with a single pole in the center of the plate (0,0) was created in order to try to study the effects of a polar stacking sequence on laminate properties and mechanical behavior. The panel was to be tested using the Instron test machine, however the panel was not flat after cure as discussed previously. After curing the first panel, several analyses were done in ANSYS in order to predict the deformed shape. The initial analyses were done using only a linear analysis and predicted minor deflection at the pole location. The final analysis result for the one-pole panel are pictured in Figure 28. The maximum deflection was 0.00010286 inches.

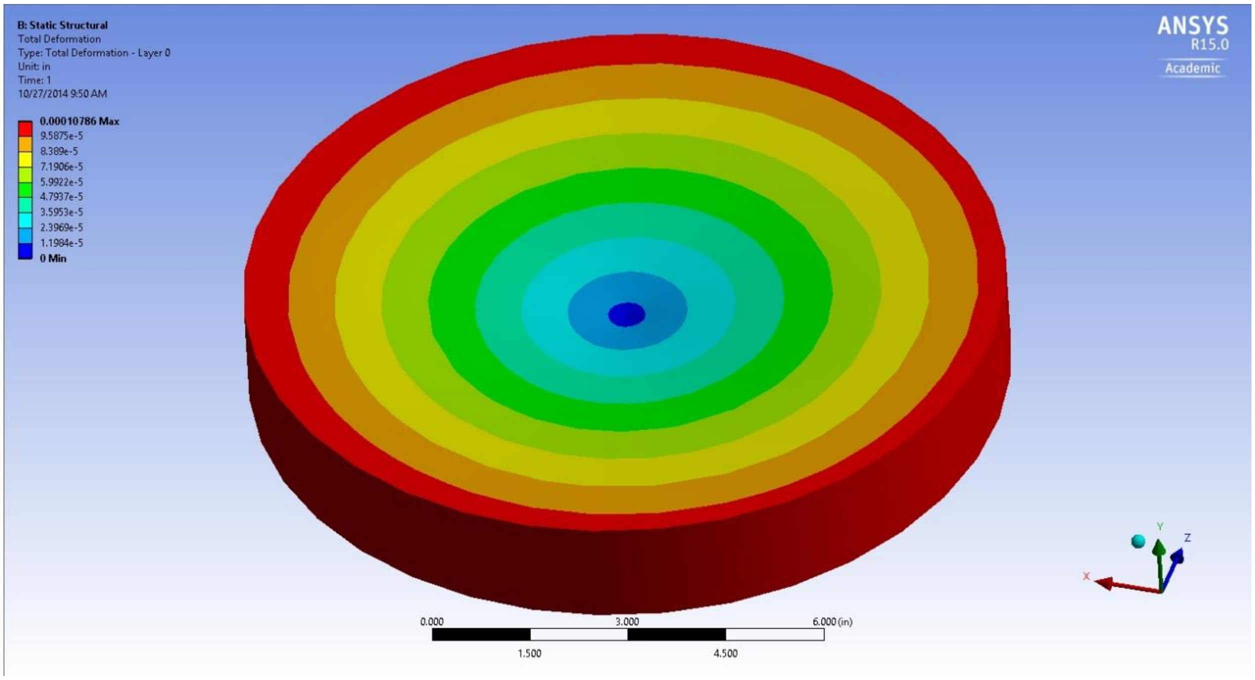

FIGURE 28: ISOMETRIC VIEW OF ONE-POLE CIRCULAR PANEL

After attempting to model the single pole panel, the two pole, circular panel was modeled and the results of initial analyses predicted insignificant deformation at the poles due to cure. The results of this analysis can be seen in Figure 29, the maximum deflection was 0.000018 inches. The initial model was done as a circle in order to simplify calculations, however the cured panel was actually two overlapped circles.

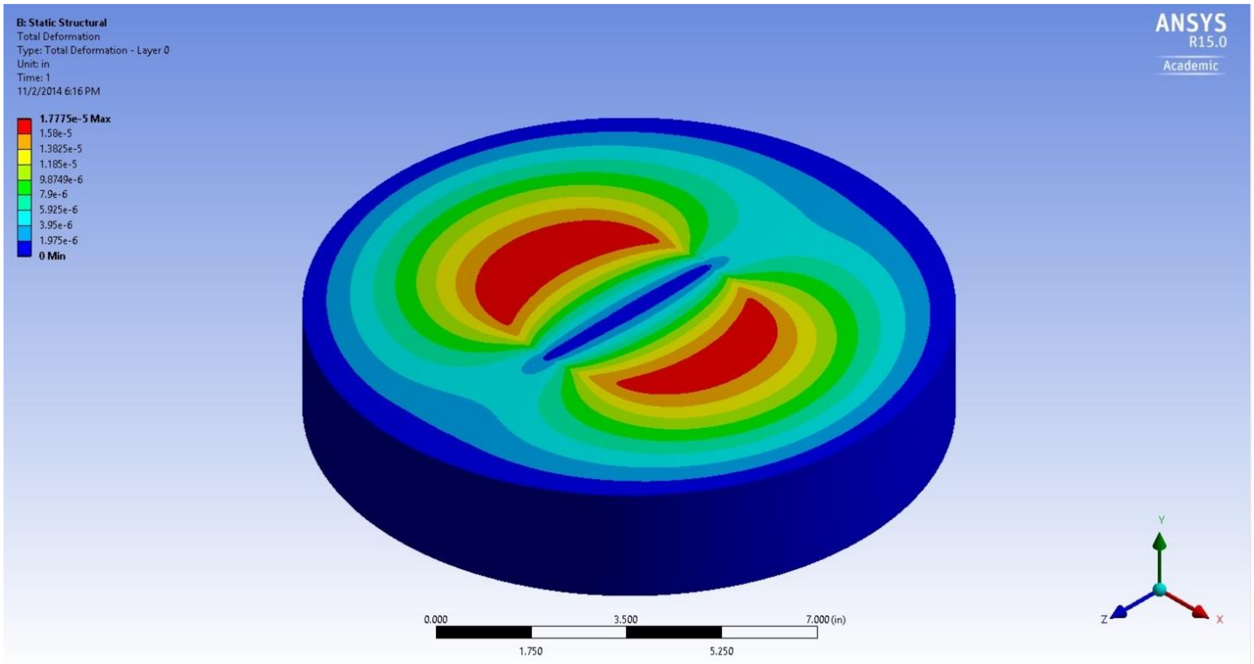

FIGURE 29: TWO-POLE Z-DEFORMATION

However, after constructing the two pole, overlapped circular panel it was apparent that the panel actually buckled with a much larger deformation than predicted. Figure 30 shows the cured shape of the two pole, circular panel.

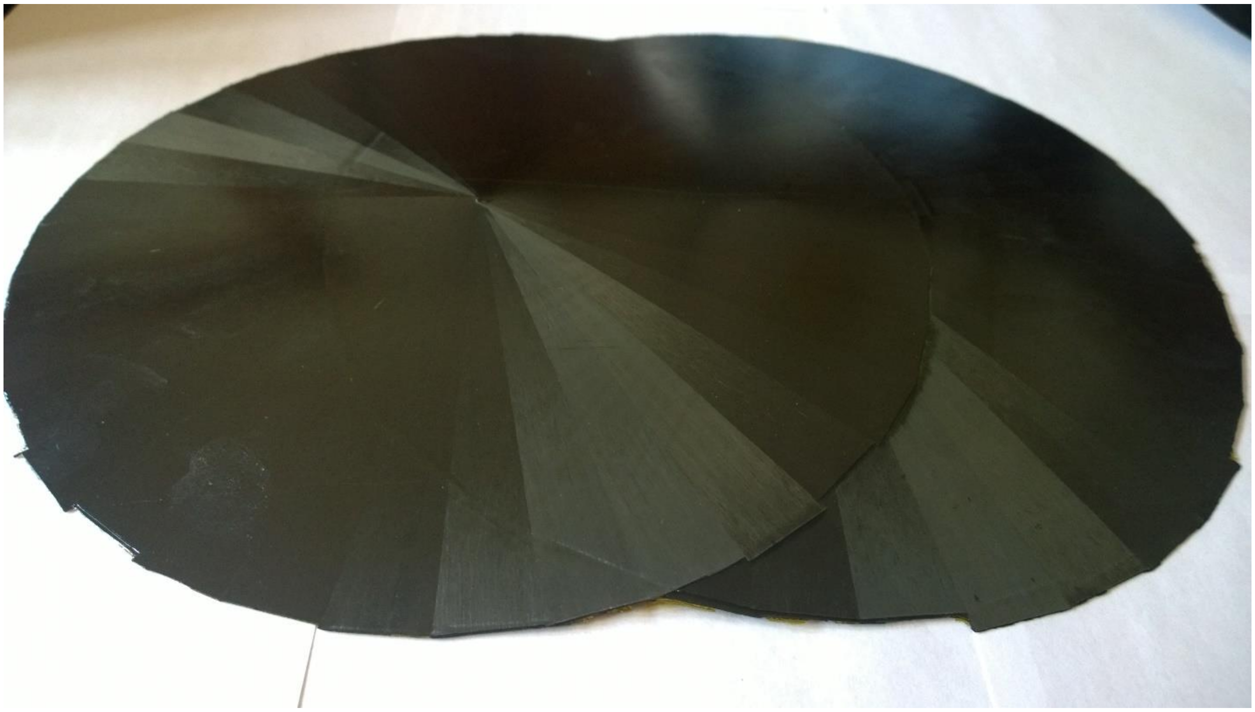

FIGURE 30: DEFORMED TWO-POLE PANEL

After these first panels and analyses, it was suggested that a two pole panel in a rectangular shape may provide more insight into these stacking sequences. The model was constructed in ANSYS and the analysis performed on a rectangular panel. The output from ANSYS can be seen in Figure 31, where the maximum deflection is 0.000252 inches and the minimum is -0.001234 inches.

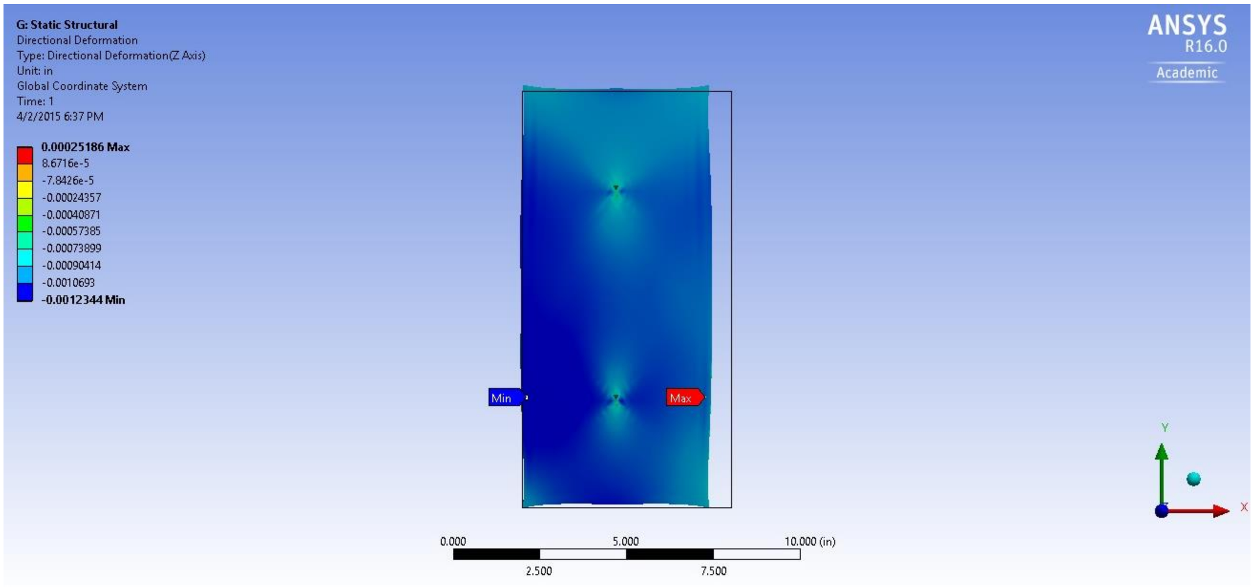

FIGURE 31: Z-DEFORMATION TWO-POLE RECTANGULAR PANEL ANALYSIS

A second two pole panel was constructed and cured as described earlier and the cured shape is shown in Figure 32.

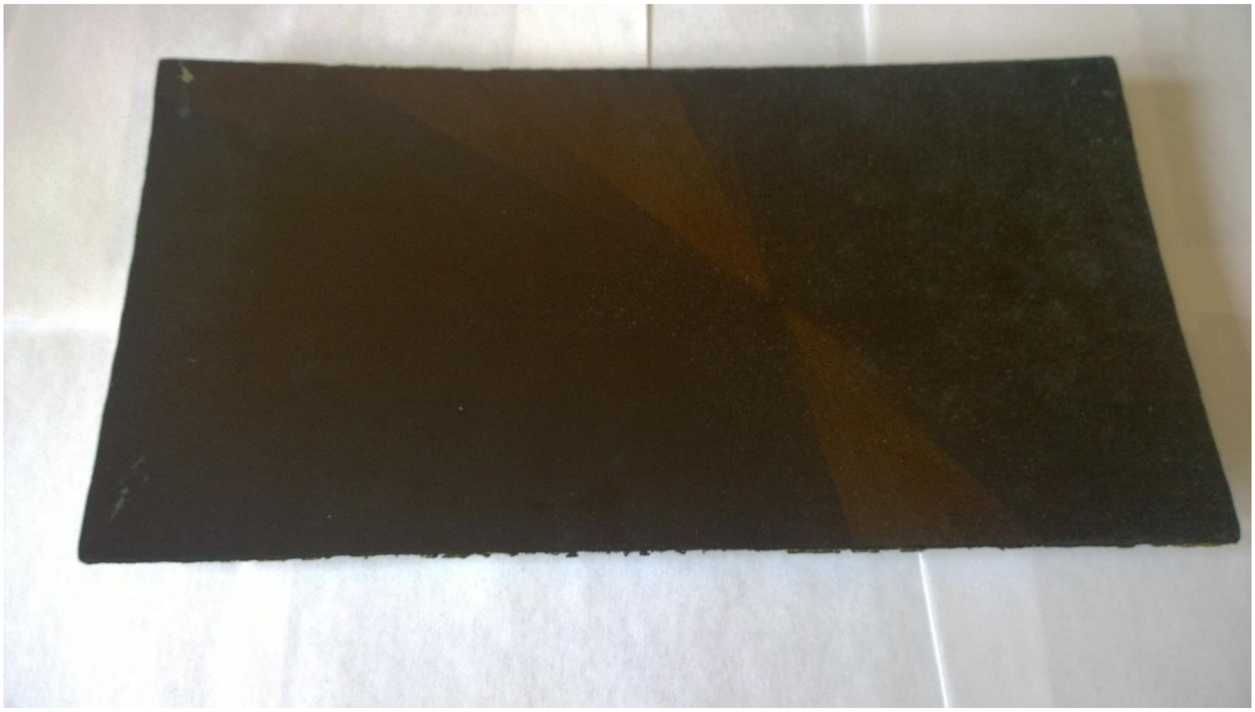

FIGURE 32: DEFORMED TWO-POLE RECTANGULAR PANEL

After curing the panel, it became apparent that the nature of the polar stacking sequences was to buckle. Therefore, more analyses, as described above, were performed to try to capture the behavior of the panels.

The eigenvalue buckling analysis resulted in a predicted buckling temperature of about 228 °F. This was confirmed with several different ΔT analyses. Table 6 shows the applied changes in temperature, from a reference temperature of 355 °F, and the corresponding λ.

**Table 6:** Shows the applied ΔT, λ, and buckling temperature for the eigenvalue analyses.

| $\Delta T$ (°F) | $\lambda$ | $T_{buckling}$ (°F) |
|---|---|---|
| 205 | 0.543 | 227.95 |
| 255 | 0.592 | 227.96 |
| 278 | 0.737 | 228.09 |

Figure 33 shows the predicted buckled shape from the eigenvalue analysis and Figure 34 shows a side view of the buckled shape. The eigenvalue analysis cannot predict the magnitude of deflection, only the deformed shape and relative magnitudes.

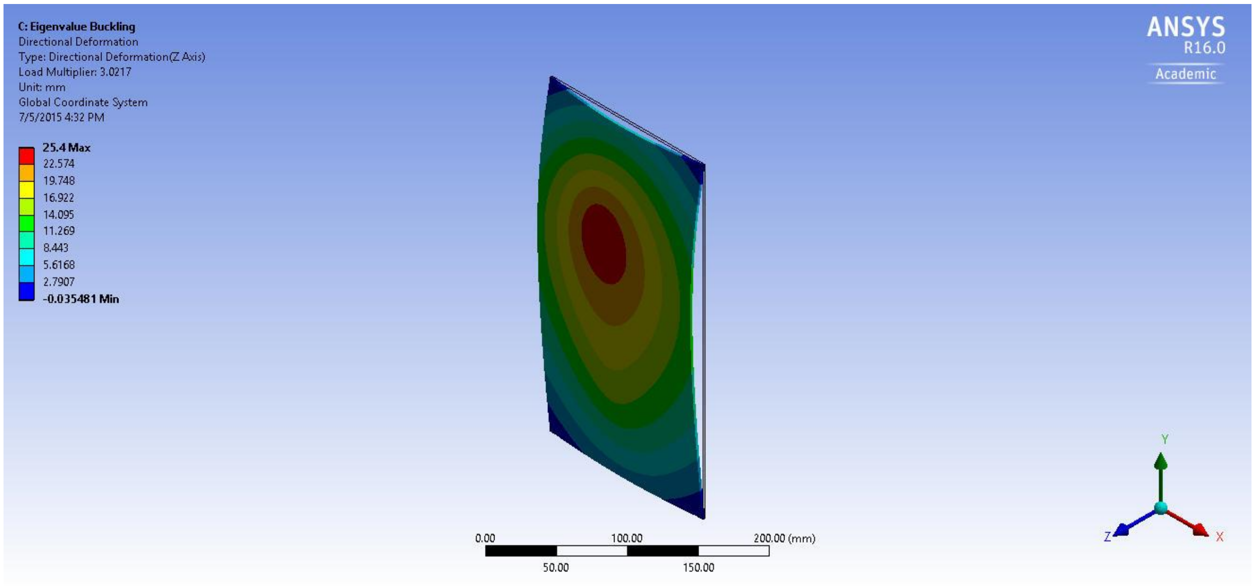

FIGURE 33: ISOMETRIC VIEW OF THE DEFORMED SHAPE OF EIGENVALUE ANALYSIS OF TWO-POLE RECTANGULAR PANEL

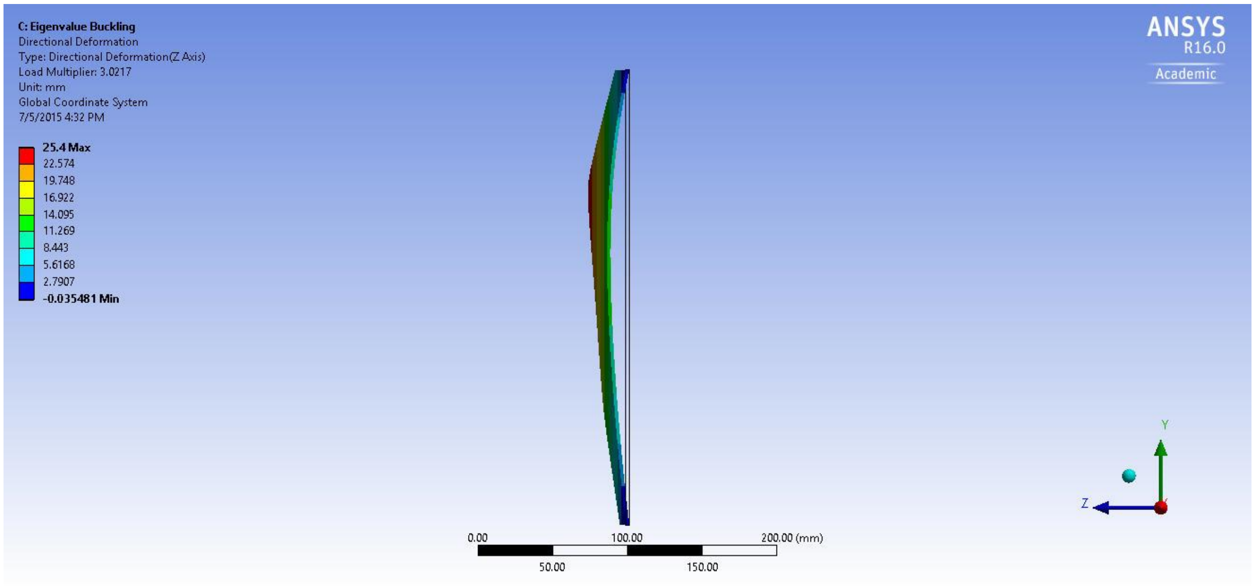

FIGURE 34: SIDE VIEW OF THE DEFORMED SHAPE OF EIGENVALUE ANALYSIS OF TWO-POLE RECTANGULAR PANEL

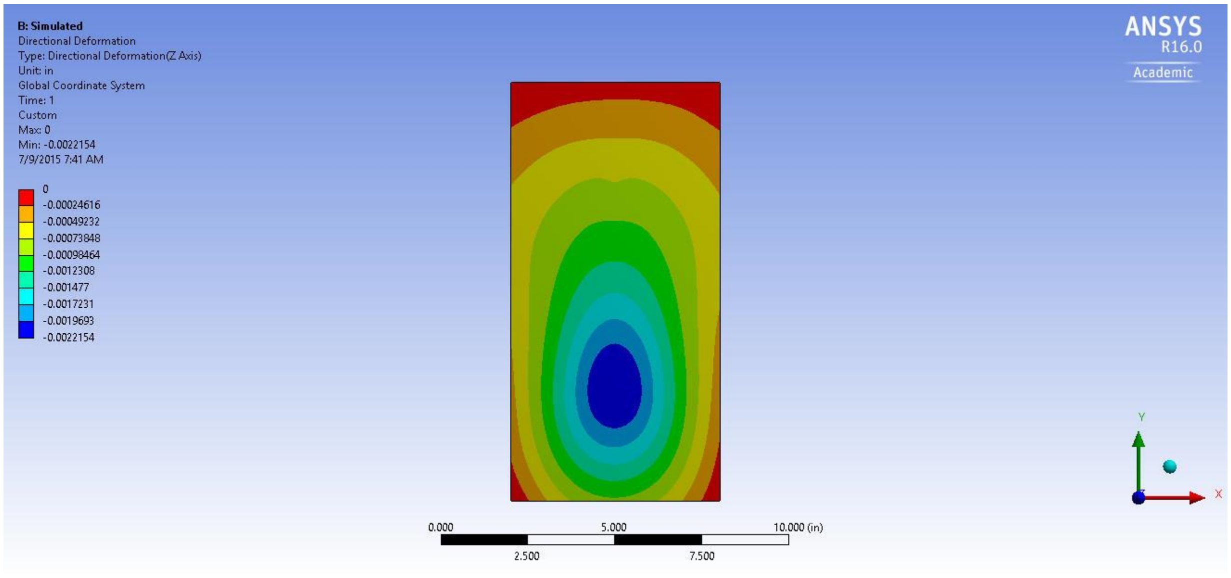

FIGURE 35: EXAMPLE Z-DIRECTION DEFORMED SHAPE FROM NON-LINEAR ANALYSIS

As mentioned previously, it was worth determining the effect modeling discontinuities into the models. Both linear and non-linear analyses were conducted on the two pole panel. Below, in Table 7, the total deformation for both types of analyses with and without the resin riches zones can be seen.

**Table 7:** Shows the total z-direction deformation ($z_{max}$+$z_{min}$) for non-linear and linear analyses with a change in temperature of -278° F with and without resin rich zones.

| | Max Z-deformation (inches) | Min Z-deformation (inches) |
|---|---|---|
| With Resin Rich | 0 | -0.0022154 |
| Without Resin Rich | 0 | -0.0028876 |

The results of the DIC analysis can for the cured shape of the panel can be seen in Figure 36. Note that the maximum value is only half of the total deformed shape, as DIC references the image in both positive and negative z-directions. Therefore the total z-value for the cured panel is 11.2 mm or 0.436 inches.

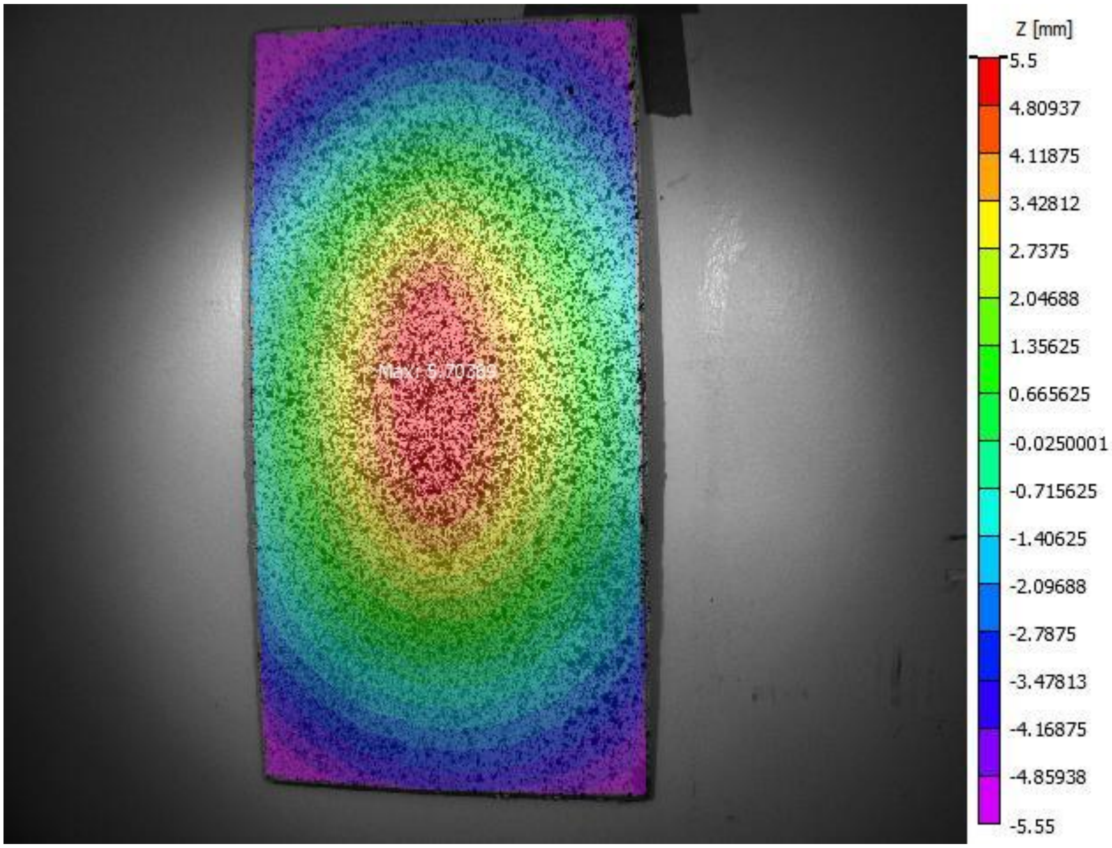

FIGURE 36: TWO-POLE RECTANGULAR PANEL DIC

## Dome

A preliminary CLT analysis was performed on the dome. Figure 37 shows the predicted hoop strains normalized by pressure at various latitude positions on the dome. It is worth noting that the hoop strains vary significantly and this reflects the changes in stiffness due to fiber angle around the dome.

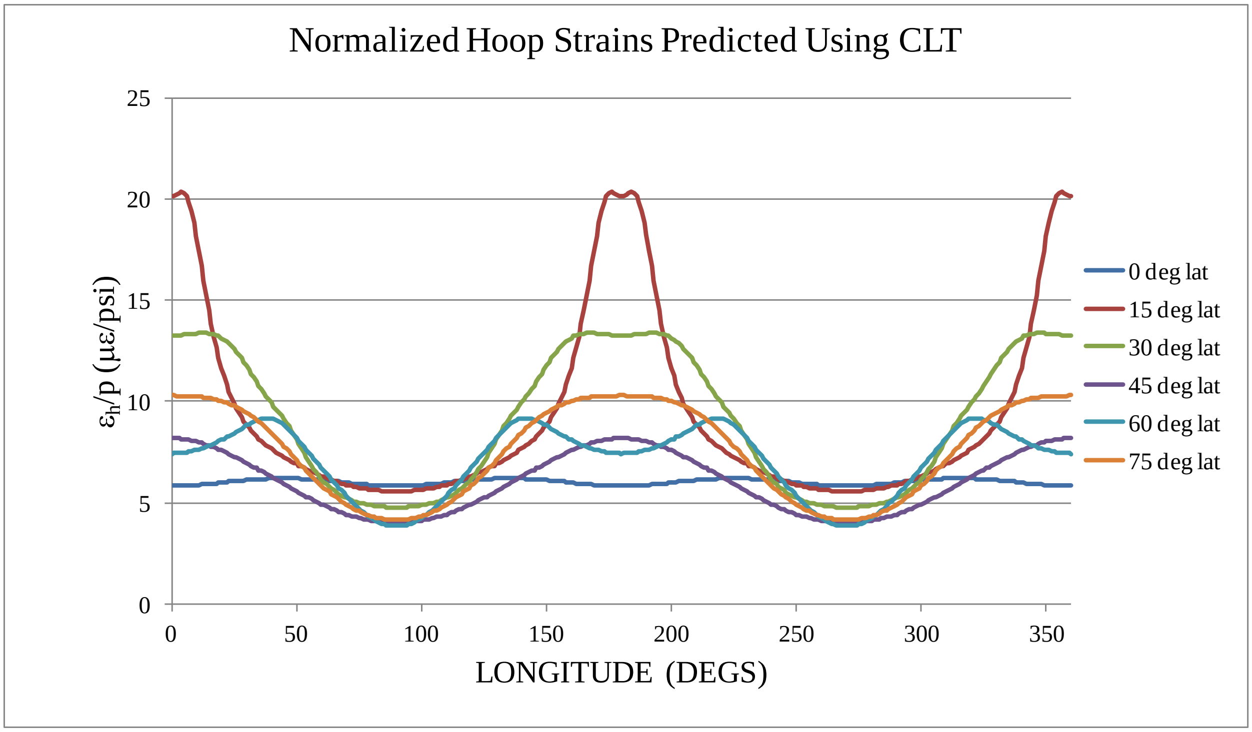

**FIGURE 37: EXPECTED HOOP STRAINS ON DOME**

The results from the dome analysis with the thermal condition are shown below. Figures 38, 39, and 40 shows the x-, y-, and z-direction deformation respectively of a standard linear static structural analysis. Figure 41 shows the expected total buckled shape as calculated by an eigenvalue analysis. The load factors output are the same for directional deformation outputs and the total deformation output, so only total deformation is shown here. The first load factor for this analysis was -1589.5 which results in a buckling temperature of 442236°F. The dome will not buckle due to any reasonable cure cycle.

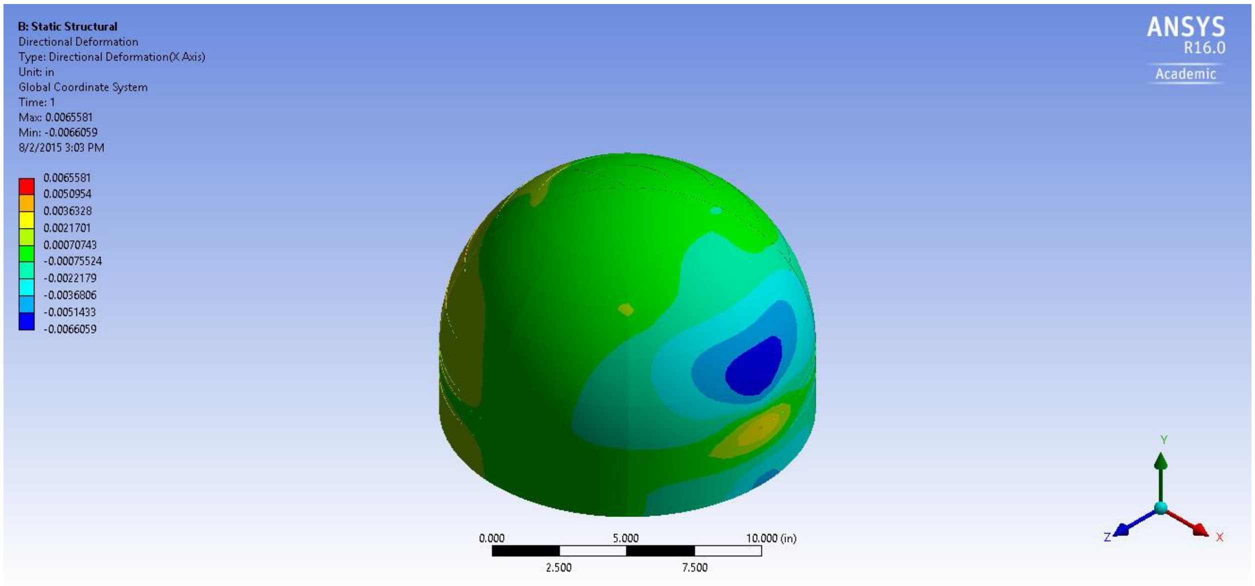

FIGURE 38: X-DIRECTION DEFORMATION OF DOME

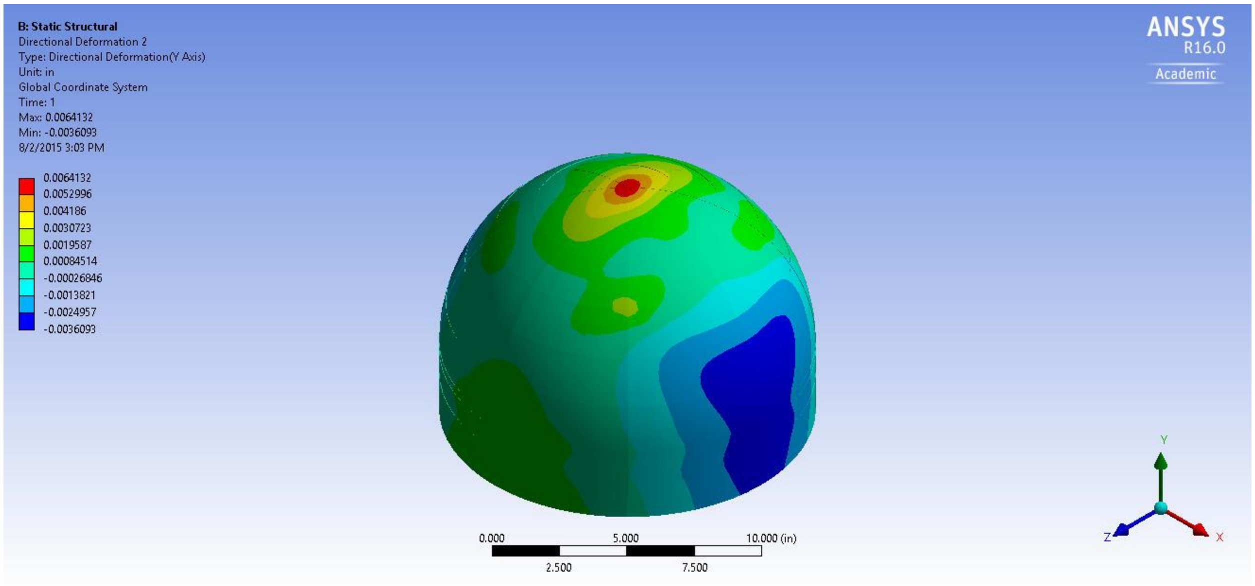

FIGURE 39: Y-DIRECTION DEFORMATION OF DOME

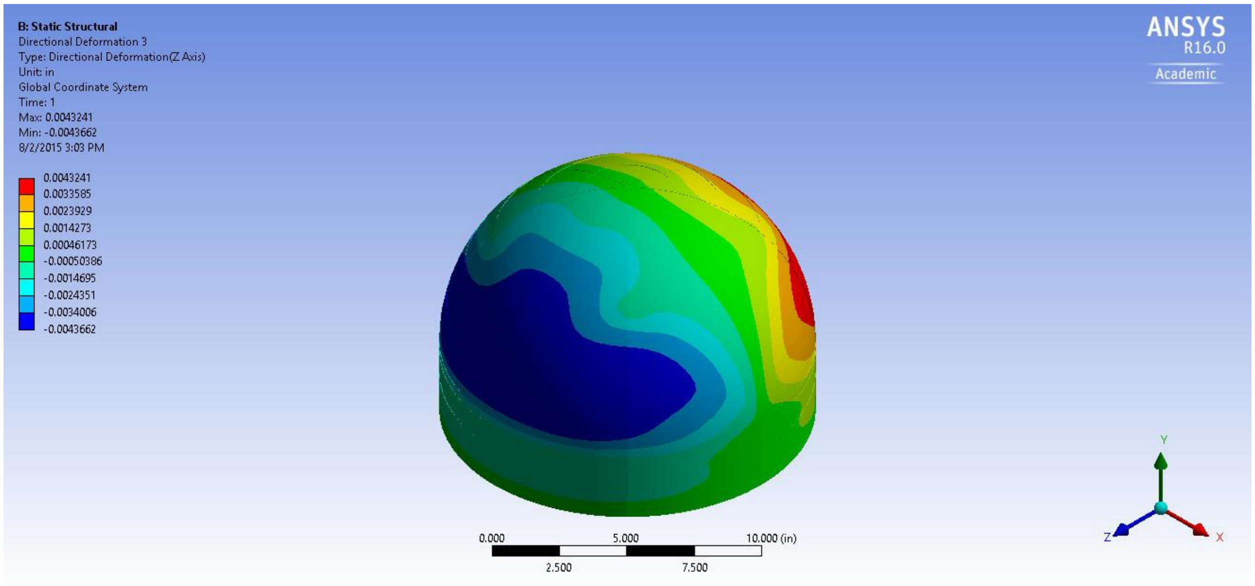

FIGURE 40: Z-DIRECTION DEFORMATION OF DOME

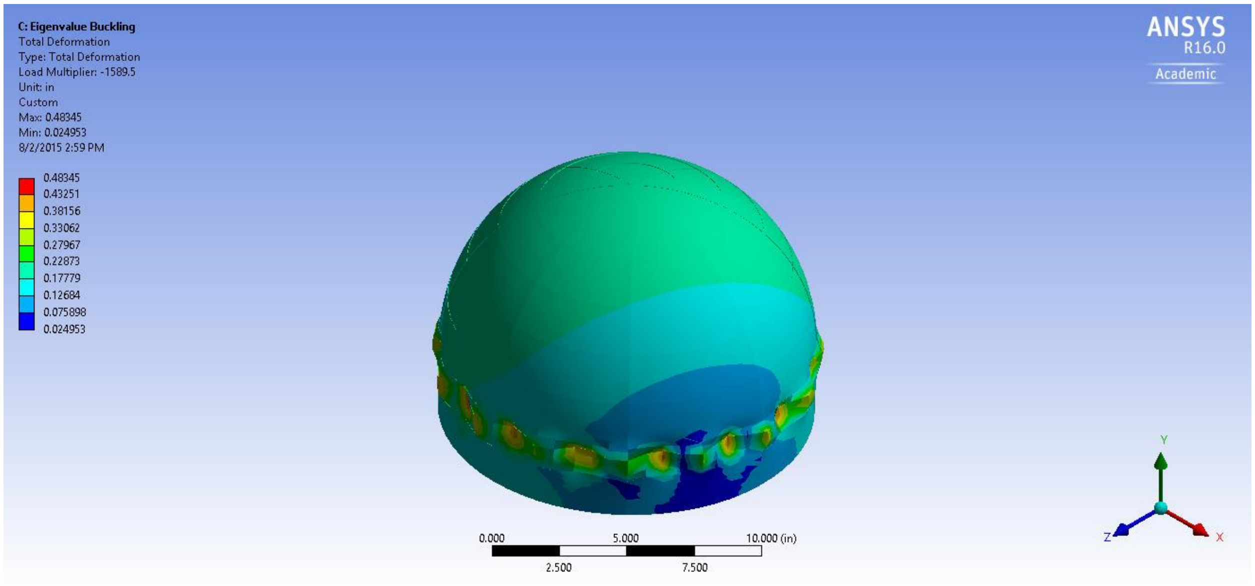

FIGURE 41: EIGENVALUE ANALYSIS TOTAL DEFORMATION

A typical strain measurement taken from the resistance strain gauges is shown in Figure 42. The pressure was increased from 0 psi to 48 psi, no audible cracking or other damage was observed. The output strains started at 0 microstrain, increased linearly, and then returned to 0 microstrain. These measurements were repeatable over many pressure cycles.

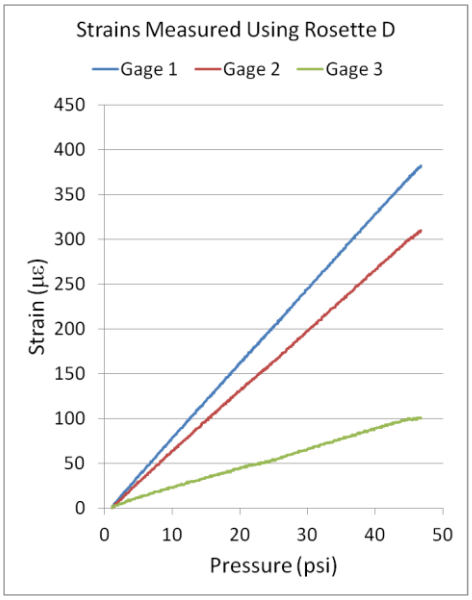

FIGURE 42: ROSETTE D STRAINS, BONDED AT (45°/0°)

The dome analyses were run at 50 psi and the hoop strains were output at every 15° latitudinal line. The output hoop strains were then normalized against pressure to be comparable with the CLT predictions and the fiber optic strain gauge measurements. The following figures (Figures 43-47) show the hoop strain at each 15° increment. The figures also contain the measurements taken with the fiber optic strain gauge and the CLT predictions.

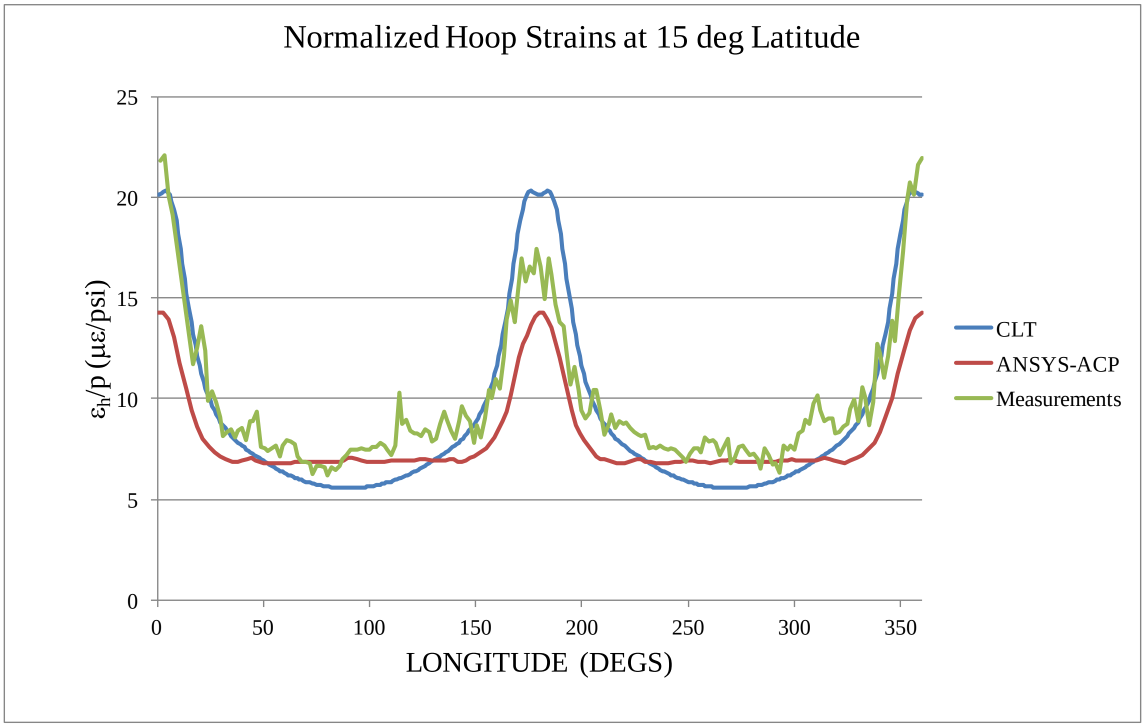

FIGURE 43: 15° LATITUDE STRAINS

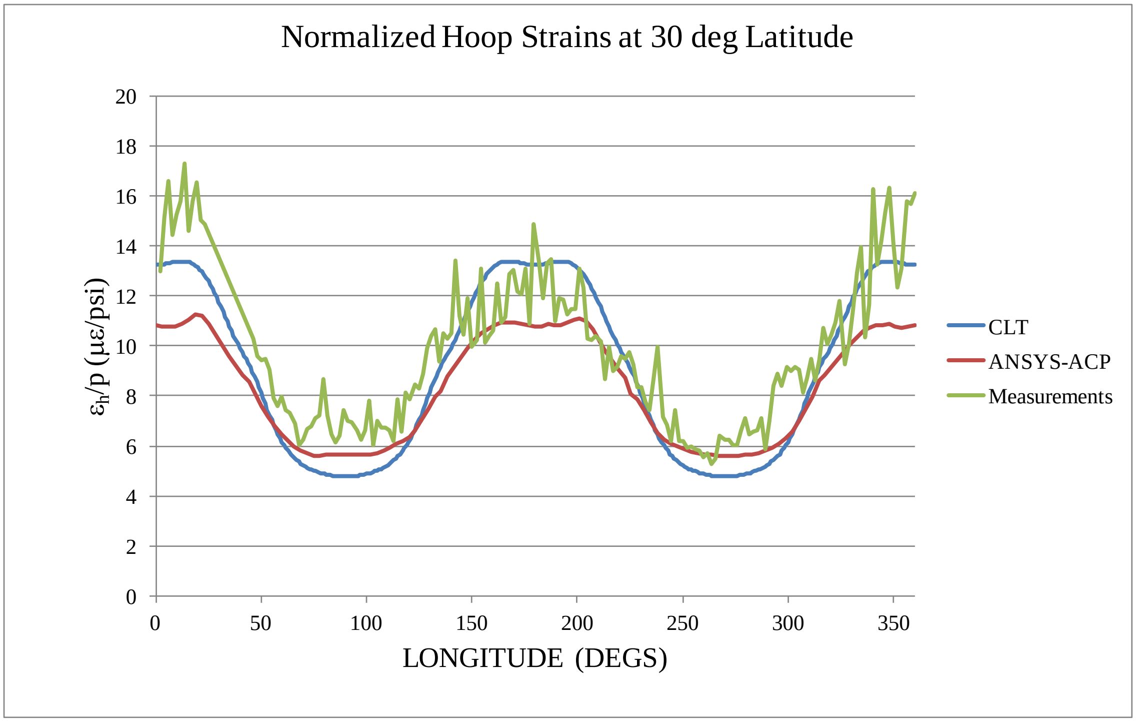

FIGURE 44: 30° LATITUDE STRAINS

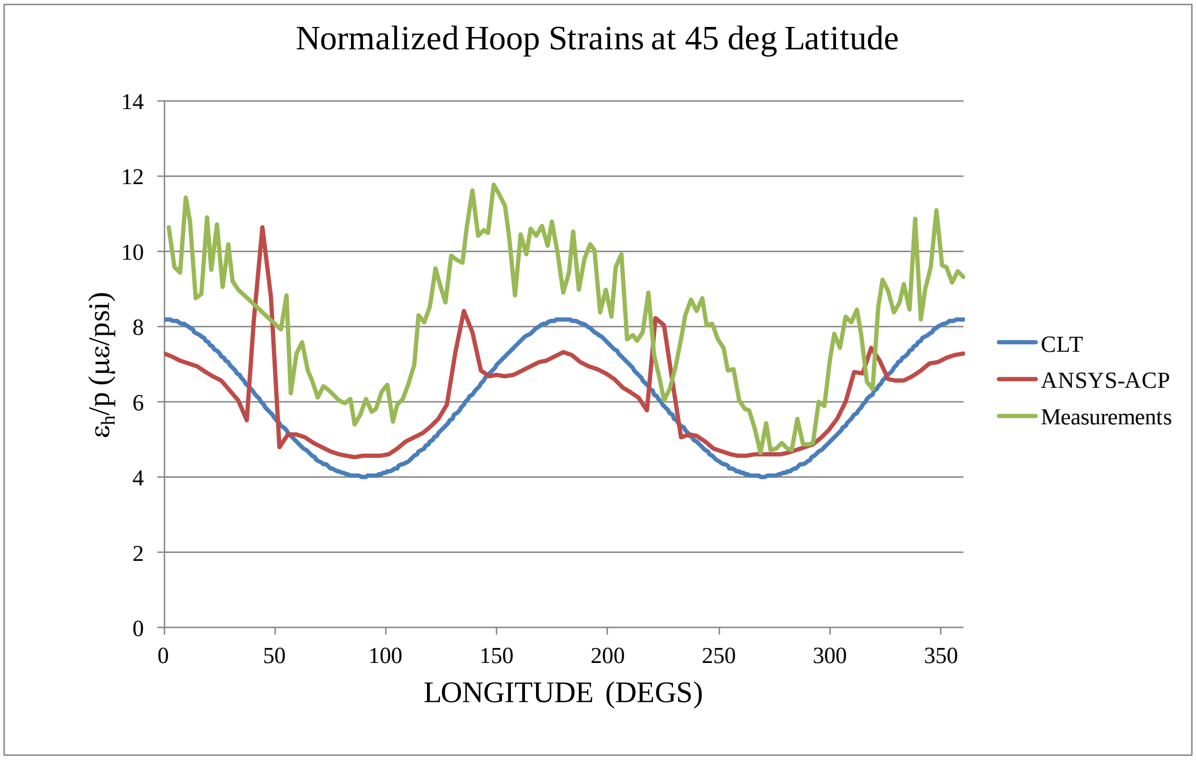

FIGURE 45: 45° LATITUDE STRAINS

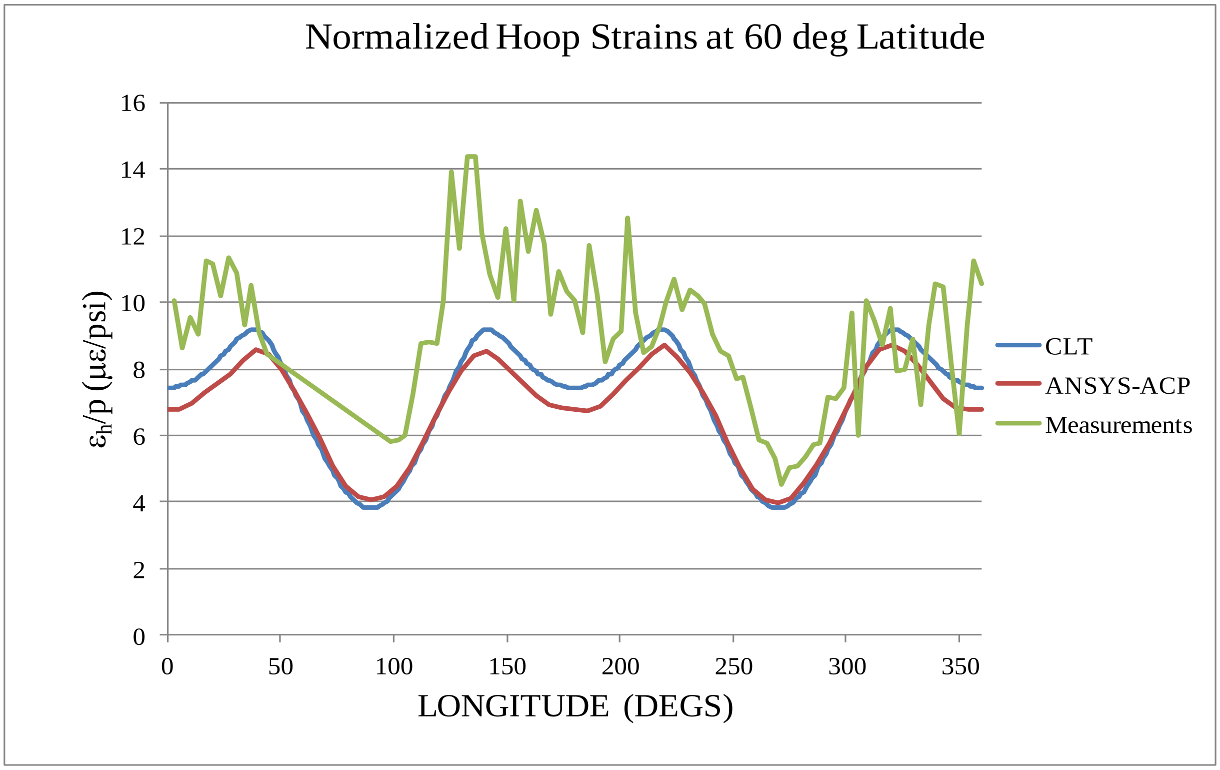

**FIGURE 46: 60° LATITUDE STRAINS**

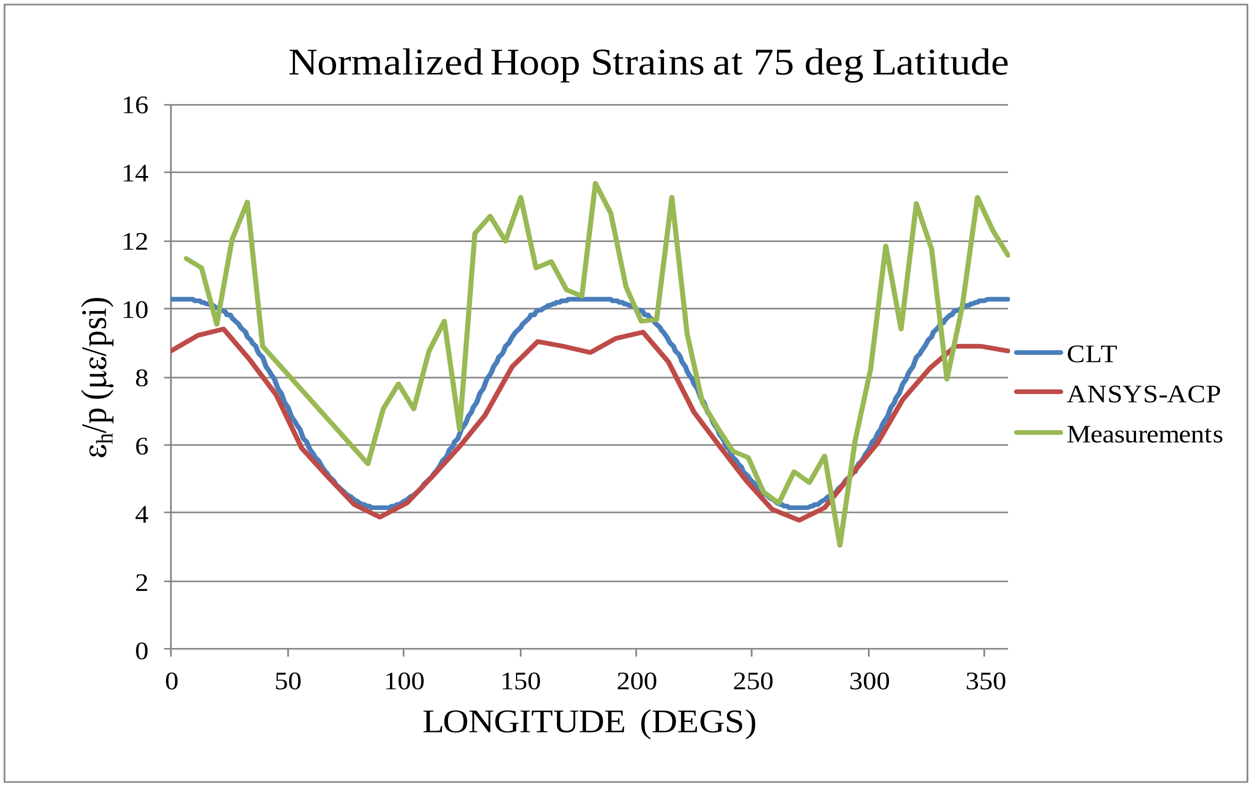

**FIGURE 47: 75° LATITUDE STRAINS**

Figure 48 shows an example of how the strains were output from ANSYS Workbench.

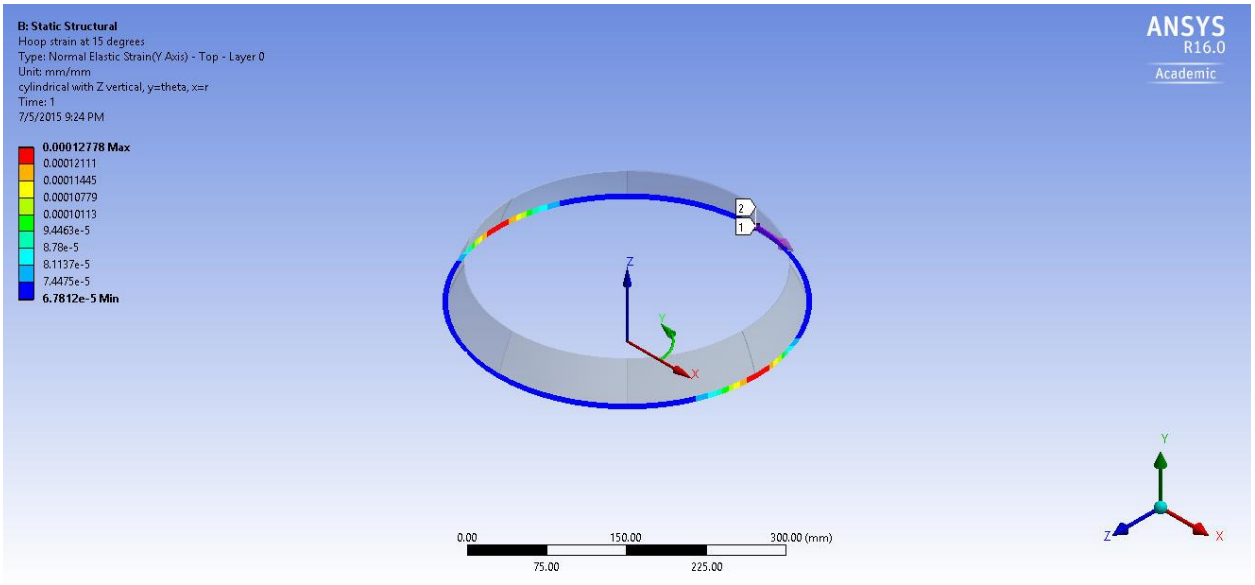

FIGURE 48: EXAMPLE HOOP STRAIN OUTPUT AT 15° LATITUDE

The dome plug, which was used to make the mold for the dome, was measured with a CMM to determine how spherical it was after curing and then the dome was measured to determine how close to spherical it was as well. Table 9 shows the form error as calculated by the software when compared to the equation of a sphere for data collected with 5 points, 10 points, 20 points, and 40 points for the plug. After measuring the plug, it was apparent that ten data points was sufficient for measuring a sphere and therefore the dome was measured three times with five point and then seven times with ten points. The results for measuring the dome are shown in Table 10.

**Table 9:** Shows the error in inches of the diameter of the foam plug as calculated by the CMM software when compared to the equation for a sphere.

| Number of Data Points | Form Error (inches) | Diameter (inches) |
|---|---|---|
| 5 | 0.0012 | 14.2248 |
| 5 | 0.0095 | 14.0381 |
| 5 | 0.0071 | 14.1619 |
| 10 | 0.0202 | 13.9637 |
| 10 | 0.0092 | 13.9590 |
| 10 | 0.015 | 13.9652 |
| 20 | 0.021 | 13.9800 |
| 20 | 0.0176 | 13.9692 |
| 40 | 0.0184 | 13.9793 |

**Table 10:** Shows the error in inches of the diameter of the dome as calculated by the CMM software when compared to the equation for a sphere.

| Number of Data Points | Form Error (inches) | Diameter (inches) |
|---|---|---|

| | | |
|---|---|---|
| 5 | 0.0059 | 14.1509 |
| 5 | 0.0036 | 13.9819 |
| 5 | 0.0045 | 14.0232 |
| 10 | 0.0241 | 14.0049 |
| 10 | 0.0141 | 13.9963 |
| 10 | 0.0129 | 13.9833 |
| 10 | 0.0250 | 13.9841 |
| 10 | 0.0189 | 14.0263 |
| 10 | 0.0345 | 14.0142 |
| 10 | 0.0078 | 14.0037 |

The average of the form error for the dome with ten data points was 0.0196 inches and the average diameter measured for the dome with ten data points was 14.0018.

The results from the DIC measurements are shown below at 48.14 psi. The first set representation of the DIC images shows each section captured side by side with a slight wrap to it indicating how the sections go together with the left and right most sides wrapping around the dome and touching. The second set of figures show the same data but stretched and fit together as a Mercator style projection (the same common style used frequently in maps).

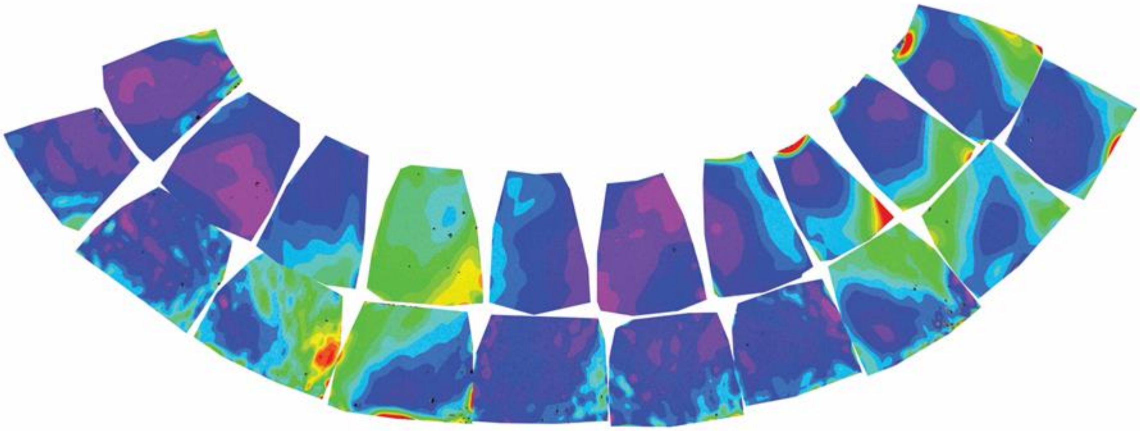

FIGURE 49: MAX PRINCIPAL STRAIN FROM DIC IN SECTIONS

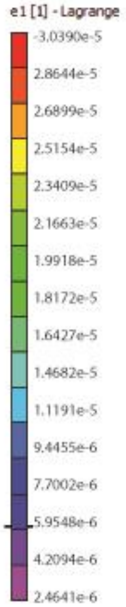

**FIGURE 50: SCALE FOR MAX PRINCIPAL STRAIN IN FIGURE 49 AND 53**

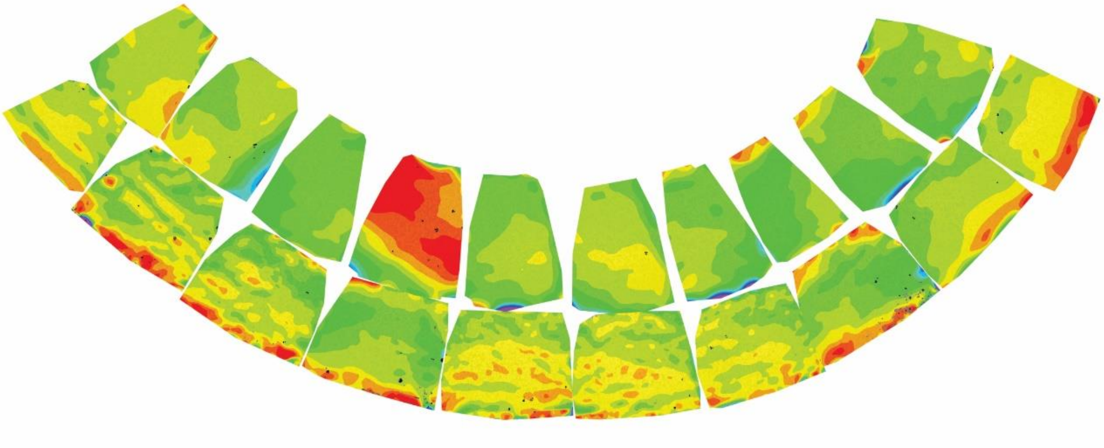

**FIGURE 51: MIN PRINCIPAL STRAIN FROM DIC IN SECTION**

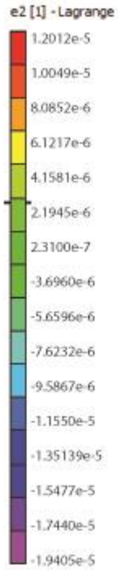

**FIGURE 52: SCALE FOR MAX PRINCIPAL STRAIN IN FIGURE 51 AND 54**

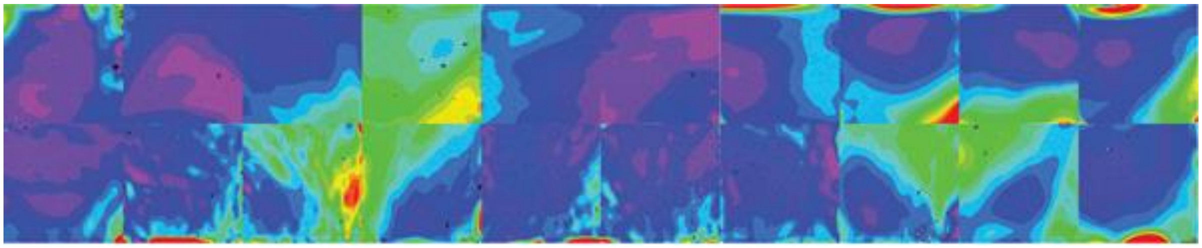

**FIGURE 53: MAX PRINCIPAL STRAIN MERCATOR MAP PROJECTION**

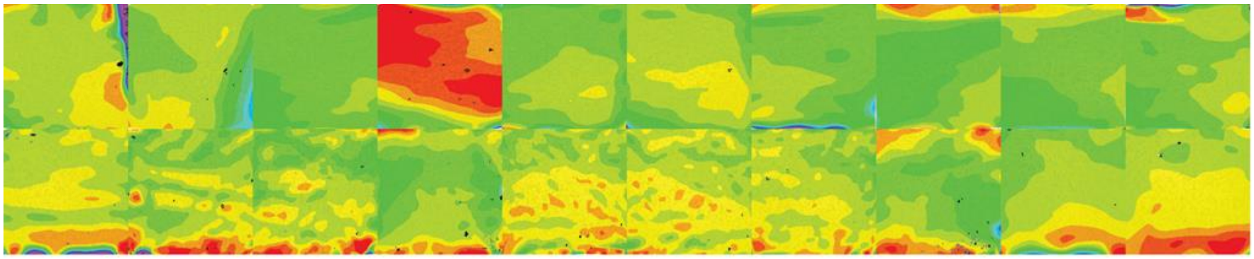

**FIGURE 54: MIN PRINCIPAL STRAIN MERCATOR MAP PROJECTION**

In order to have something to compare these DIC results to, similar images were extracted from ANSYS and arranged as a Mercator projection. It is worth noting here that the scales used for ANSYS and DIC do not match up perfectly due to noise.

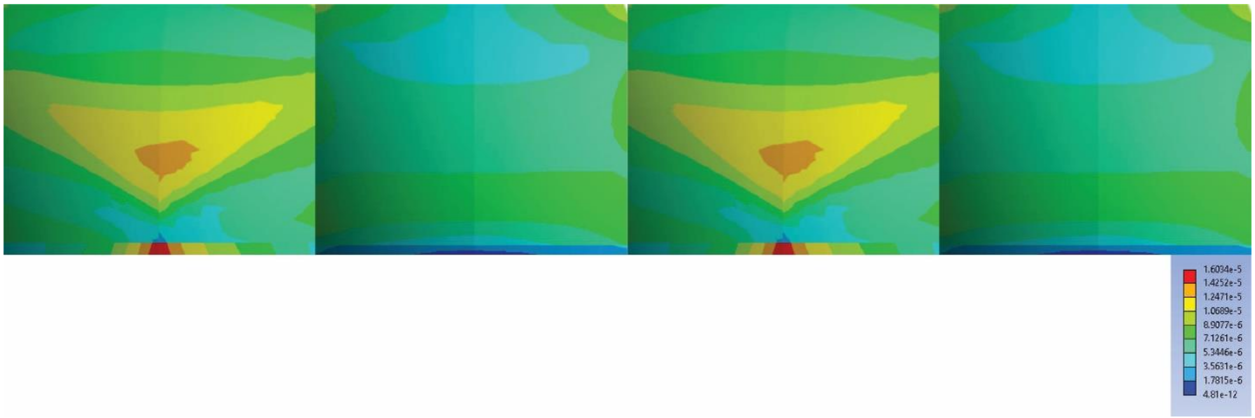

FIGURE 55: MAX PRINCIPAL STRAIN FROM ANSYS, MERCATOR MAP PROJECTION

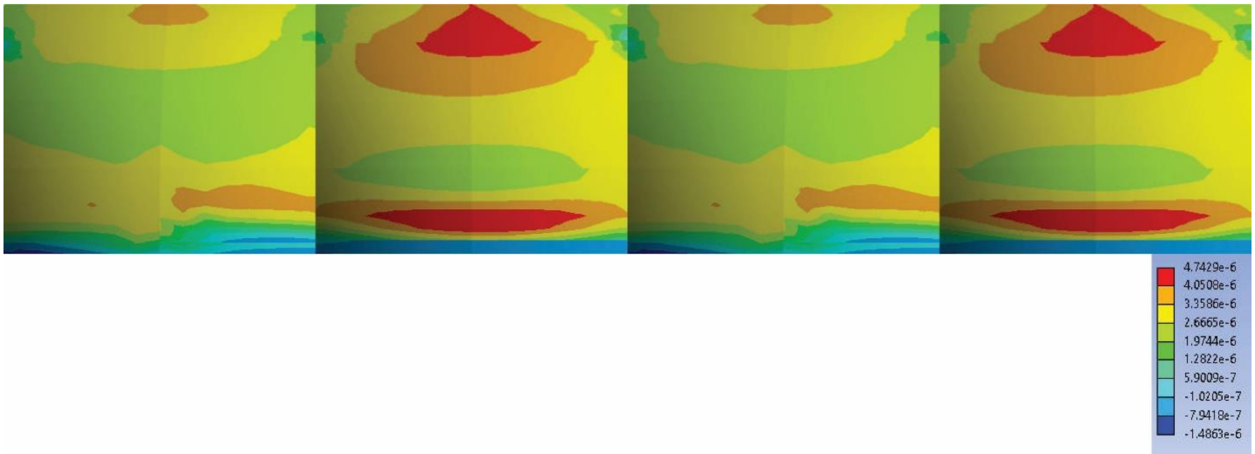

FIGURE 56: MIN PRINCIPAL STRAIN FROM ANSYS, MERCATOR MAP PROJECTION

## Discussion

After curing the one-pole, circular panel, it became apparent that the panel did not cure flat. The panel could be popped back and forth between two stable positions with the deformed shape being equal in magnitude but flipping between positive and negative out of plane deformation. This was due to the mismatch in coefficients of thermal expansion between the fibers and the epoxy, but it specifically was caused by the compressive residual stresses in the tangential direction around the plate. These arose because the epoxy would contract significantly more during cure than the fibers resulting in the buckled, conical shape. The ANSYS analysis for the single pole plate predicted a low deformation due to the curing process (z = 0.000168 inches) which did not match the deformed shape as seen after cure.

The same phenomenon occurred when the two-pole, circular panel was constructed and cured, however out of fear of breaking the panel, it was not popped back and forth through the stable positions. Similarly, the ANSYS analyses performed did not predict an accurate deformation out of plane (z = 0.000018 inches).

Finally, the two pole, rectangular panel resulted in the same general shape with the poles popping up out of plane. At this point, it was concluded that making a flat plate with a polar stacking sequence was not reasonable. In the previous section, the CMM measurements for the two pole, rectangular panel are shown (z = 0.622 inches). The results taken from the CMM are the true cured shape measurements. When compared with the DIC results, z = 0.436 inches, they differ significantly from the CMM values. This difference is most likely due to the panel being adhered to a vertical wall and viewing the panel from an angle offset from perpendicular to the surface. However the results confirmed that the speckling pattern and sizing were adequate for a part of that size and therefore would be adequate for the dome. The most significant results from the ANSYS analyses performed are those of the eigenvalue buckling analysis. As can be seen from the results above, both the linear and nonlinear analyses fail to accurately predict the magnitude of the deformed shape of the panel. In fact they are off by several orders of magnitude. However, the results from the eigenvalue buckling analysis confirm that the panel buckled during cure and predicted that buckling would occur around 228° F during the cooling process. Since both the linear and non-linear analyses were not able to capture the deformation of the cured panel accurately, more research is necessary to determine whether or not ANSYS can accurately capture the deformation due to cooling the panel to room temperature.

The CMM results given in the previous section for the spherical nature of the dome confirmed that after construction and curing, the dome remained spherical to within an average of 0.0196 inches in diameter. Additionally the foam plug was measuring using the same methodology to confirm the accuracy of the CMM since the dome was CNC milled.

After applying an eigenvalue analysis to the dome, the results indicated that the dome would not buckle during cure or any realistic temperature near to cure. This again confirmed the CMM measurements that the dome remained largely spherical.

The results measured by the fiber optic strain gauge, predicted by CLT, and predicted by ANSYS for pressurization of the dome agree quite well. Qualitatively, the shape of the predicted strains around the surface of the dome at each latitude as shown in Figures 43-47 follow the same envelope closely. Largely, the differences seen in the fiber optic results are caused by noise. Additionally, at the higher latitude positions, the length of the fiber optic cable decreases, resulting in fewer data points over the dome. This causes the pronounced jumps in the measured strains on the surface.

Comparing the DIC results to the ANSYS predictions resulted in a close match between the two in terms of the scale of strains. Due to the spherical nature of the dome, it was futile to utilize strains in the x- and y-directions because the axes changed as different sections of the dome were captured and especially so at the top of the dome. Around the sides of the dome, the x-direction in DIC would correlate well to the hoop strains on the surface of the dome, however at the top of the dome, this was no longer the case. Therefore, the principal strains on the surface of the dome were examined with DIC and ANSYS. In the DIC software used (VIC 3D), only a maximum and minimum principal strain was available because the software does not have any information through the thickness. In ANSYS, through the thickness strains are known and therefore maximum, middle, and minimum principal strains are available for output. This caused some confusion until ultimately it was determined that the minimum principal strain as output by ANSYS was actually the through-thickness strain and thus not valuable in comparing to the results collected from DIC techniques. Once all of the problems were worked though, it could be seen that indeed, both ANSYS and DIC predict and measure strains within the same range (the strains shown above in Figures 47, 49, 51, 52, 53, and 54 are normalized by pressure, so they represent the strain present per one pound per square inch) of approximately 6 microstrain to 25 microstrain for the maximum principal strain and about -17 microstrain to 10 microstrain for the minimum principal strain. The scales shown for the DIC results exceed both of these ranges, but this was due to noise captured by DIC. The was another large problem with comparing DIC to anything else because the noise spreads out the scale and when the scale was spread that large for the ANSYS analyses, the data became almost uniform.

Some of the buckling that was observed in the panels could be due to the previously mentioned overlap along the edges of the triangles and at the poles when stacking the plies. Placing each triangle precisely on top of the previous layer proved to be difficult and placing the triangles such that they meshed perfectly around the entire plate proved impossible. However, the effect due to these overlaps was likely very small, but impossible to quantify without making a ‘perfect’ polar stacking sequence panel.

## Conclusions

From the analyses performed and the flat plates built, two things can clearly be seen. First was that creating a flat plate using the polar stacking sequence described in this document cannot be done by the methods used here. Second was that ANSYS was unable to predict the magnitude of the buckled shape accurately with either a linear or nonlinear analysis. The reason for the buckling of the plates was the mismatch in coefficients of thermal expansion between carbon fibers and epoxy resin generally. In particular, the mismatch caused a compressive tangential strain around the plate, forcing the pole locations to peak and deform out-of-plane during cure. The reason ANSYS was unable to predict the magnitude of the buckled shape was likely due to the unique stacking sequence, nonsymmetric nature of the panel, and standard calculations necessary to analyze a panel with a polar stacking sequence do not exist. Due to the other tests performed in conjunction with ANSYS analyses (using CLT and SPORTHO), the author was confident that ANSYS can accurately capture simpler stacking sequences using standard lay-up practices.

After measuring the dome for its spherical-ness using a CMM, checking for buckling using ANSYS, and pressurizing the dome, the original question about strength to weight ratios of this polar stacking method was never answered. It was determined that the more basic question, “Can the behavior of a flat plate or curved surface constructed in this way be predicted?", was first necessary to answer. Measuring the dome for how far from spherical it was yielded good results at less than two tenths of a percent difference from the equation for a perfect sphere. And the ANSYS eigenvalue analysis ran predicted that no buckling would occur during cure. Qualitatively, the shape of a panel after curing can be predicted using an eigenvalue analysis, however the quantitative amount cannot. The strains caused in the surface of a hemispherical dome can be reasonably well predicted using a linear analysis in ANSYS ACP. Additionally, DIC can capture within the same scale the strains on the surface of the fourteen inch diameter dome readily and they can be compared to the strain field produced by ANSYS. All this says, more research could be done here.

More work should be performed in order to fully understand this phenomenon and better enable ANSYS users to capture cure cycles, particularly of nonsymmetric stacking sequences. There is large potential for using the methods described here for many applications in aerospace and other fields, however there are more questions left with an 'incomplete' or no answer before applying this technology to commercial use. Pressurization and linear analysis performed by ANSYS agree reasonably well and cure cycles and nonlinear analyses are more variable in quality as previously known. It is the authors recommendation that more work be done to study different combinations of boundary conditions that could be used to simulate the cure cycle, what are the results after studying this stacking sequence in light of failure criterion, and what is the strength to wait ratio of this stacking sequence compared to a standard draped layup?

# Literature Cited

[1]. Agarwal, B., Broutman, L., & Chandrashekhara, K. (2006). *Analysis and Performance of Fiber Composite* (3rd ed.). Hoboken, New Yersey: John Wiley and Sons.

[2]. ASTM D3039 / D3039M-14, “Standard Test Method for Tensile Properties of Polymer Matrix Composite Materials”, ASTM International, West Conshohocken, PA, 2014, www.astm.org

[3]. B Pan, “Study on Subset Size Selection in Digital Image correlation for Speckle Patterns,” *Optics Express*, vol. 16, no. 10, 7037-7048, 2008.

[4]. Malick, P K. (1993). *Fiber Reinforced Composites: Materials, Manufacturing, and Design.* Marcel Dekker, Inc.

[5]. Chawla. Krichan K. (1998). *Composite Mateirals: Science and Engineering (*2nd ed). Springer.

[6]. Crothers, P J, Drechsler, K Feltin, D. Herszberg, I and Bannister M. “The Design and Application of Tailored Fiber Placement.” Proceedings of ICCM11, Gold Coast, Australia, Vol 1. 14-18. July (1997), pp 600-610.

[7]. Dano, Marie-Laure, and Michael W. Hyer. "Thermally-induced Deformation Behavior of Unsymmetric Laminates." *International Journal of Solids and Structures* 35.17 (1998): 2101-120. *Elsevier Science LTD*. Web. 29 Apr. 2015.

[8]. Dano, M. L., and Hyer, M. W., "The Room-Temperature Shape of General Unsymmetric Laminates." *Proceedings of the American Society for Composites Eleventh Technical Conference.* Pp 100-110. Oct 9, 1996

[9]. Eckold, Geoff. (1994) *Design and Manufacturing of Composite Structures.* McGraw-Hill, Inc.

[10]. Halpin, John C. (1980). *Primer on Composite Materials Analysis, (*2nd ed). Revised Technomic Publishing.

[11]. Hamamoto, A. and Hyer, M. W. (1987) Non-linear temperature-curvature relationships for unsymmetric graphite-epoxy laminates. *International Journal of Solids and Structures,* 23, 919-935.

[12]. Henry, T., Bakis, C., & Emerson, R. (2013). "Characterization of compressively loaded filament wound composite cylinders using digital correlation. *28th Annual Technical Conference of the American Society for Composites,* 778-795.

[13]. Hyer, M.W., "Mechanics of Unsymmetric Laminates (Ch. 2)", *Handbook of Composites*, C.T. Herakovich and Y.M. Tarnopol'skii, Elsevier Science Publishers, 2, 86- 114, 1989

[14]. Hyer, M.W., "Some Observations on the Cured Shapes of Thin Unsymmetric Laminates," *J. Composite Materials, 15: 175-194, 1981a.*

[15]. Hyer, M.W., "Calculations of the Room-Temperature Shapes of Unsymmetric Laminates," *J. Composite Materials, 15: 296-310, 1981b.*

[16]. Kuo, T., Wang, W., Chu, C., Chen, J., Hung, T., & Chang, J. (2013). "Buckling measurement of cylindrical shells by digital image correlation method." *Proceedings of the ASME 2013 International Mechanical Engineering Congress and Exposition,* 1-8. Retrieved April 29, 2015, from http://proccedings.asmedigitalcollection.asme.org/

[17]. M A Sutton, J-J Orteu and H W Shreier, Image Correlation for Shape, Motion, and Deformation Measurements. New York: Spring Science + Business Media, LLC, 2009.

[18]. McLaughlan, P., Forth, S., & Grimes-Ledesma, L. (2011). *Composite Overwrapped Pressure Vessels, A Primer.* Springfield, Virginia: NASA Center for AeroSpace Information.

[19]. B. Pan, “study on Subset Size Selection in Digital Image Correlation for Speckle Patterns,” *Optics Express,* vol 16, no. 10, pp. 7037-7048, 2008.

[20]. Peeters, L. J. B., Powell, P. C. and Warnet, L. (1996) Thermally-induced shapes of unsymmetric laminates. *Journal of Composite Materials* 30, 603-626.

[21]. Russell, S S. (1986) Applications of digital image correlation methodology to problems in composites. *Proceedings of the 1986 SEM Spring Conference on Experimental Mechanics.* P 34-41.

[22]. Schlecht, M., Schulte, K. and Hyer, M. W. (1995) Advanced calculations of the room-temperature shaes of thin unsymmetric composite laminates. *Composite Structures,* 32, 627-633.

[23]. Tuttle, M and Cross, J. *Stress Analysis of a Pressurized Composite Hemisphere.*

[24]. Tuttle, M. (2013). *Structural Analysis of Polymeric Composite Materials (*2nd ed.). Boca Raton, Florida: Taylor and Francis Group, LLC.

[25]. Yarrapragada, R., Mohan, R., & Kiran, B. (2012). “Composite pressure vessels”. *IJRET,* 1(4), 597-618. Retrieved April 29, 2015, from http://www.ijret.org

# Appendices

## Appendix A

Matlab code used to create the 3D surfaces from the CMM measurements.

```
%read in file
filename = 'random.xlsx';
coords = xlsread(filename);

%set up xyz
x = coords(:,1);
y = coords(:,2);
z = coords(:,3);

%plot specifications
bound = [-.50 6 -.50 12];
vp = [0 90];
ar = [1 1 .25];

tri = delaunay(x,y);
trisurf(tri, x, y, z);
axis image;
daspect(ar);
axis vis3d; %freezes axis so that 3d images can be rotated without messing up scale

%clean up the plot and add color
axis off;
shading interp;
colorbar EastOutside;

figure;
scatter(x,y,'filled');
axis image;
```

## Appendix B - Shows the convergence of a basic CLT analysis run on a square 12”x12” panel subject to a 100 lb/in stress resultant along the top edge.

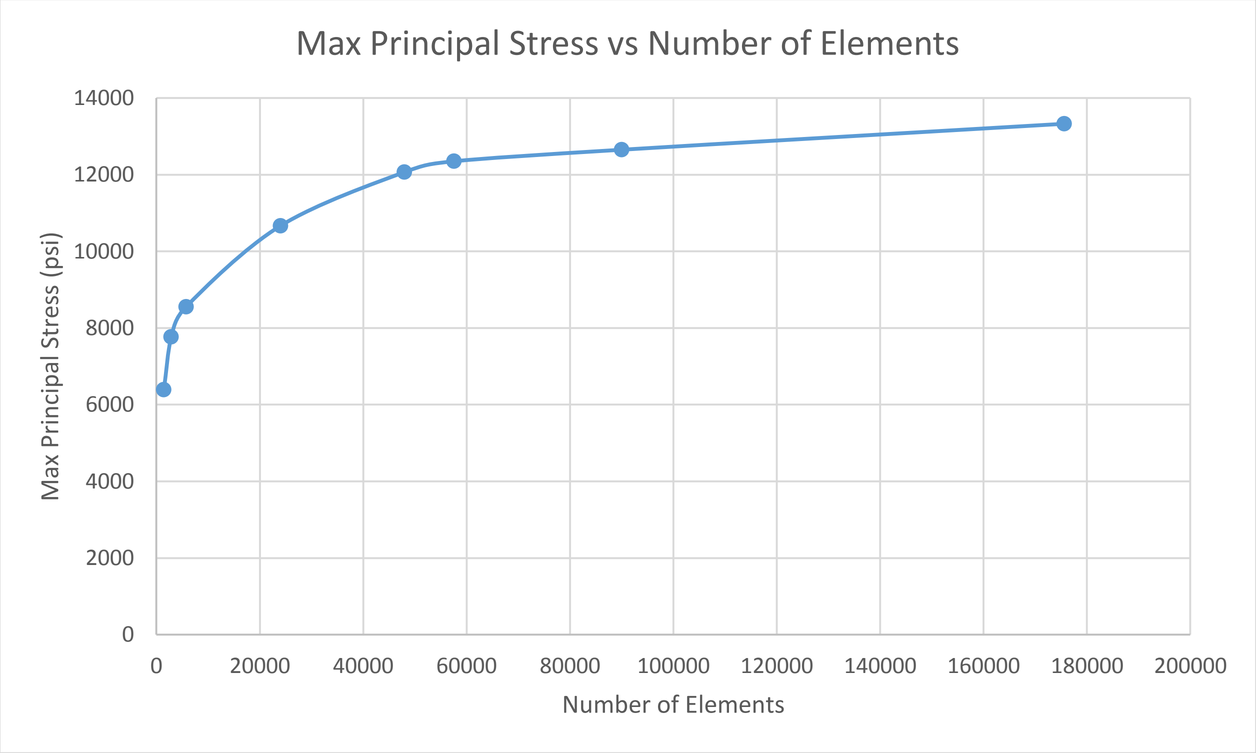

FIGURE 57: CONVERGENCE FOR CLT ANALYSIS

## Appendix C

Material Properties, Plots of Average Axial and Transverse Strain for Tensile Testing Coupons

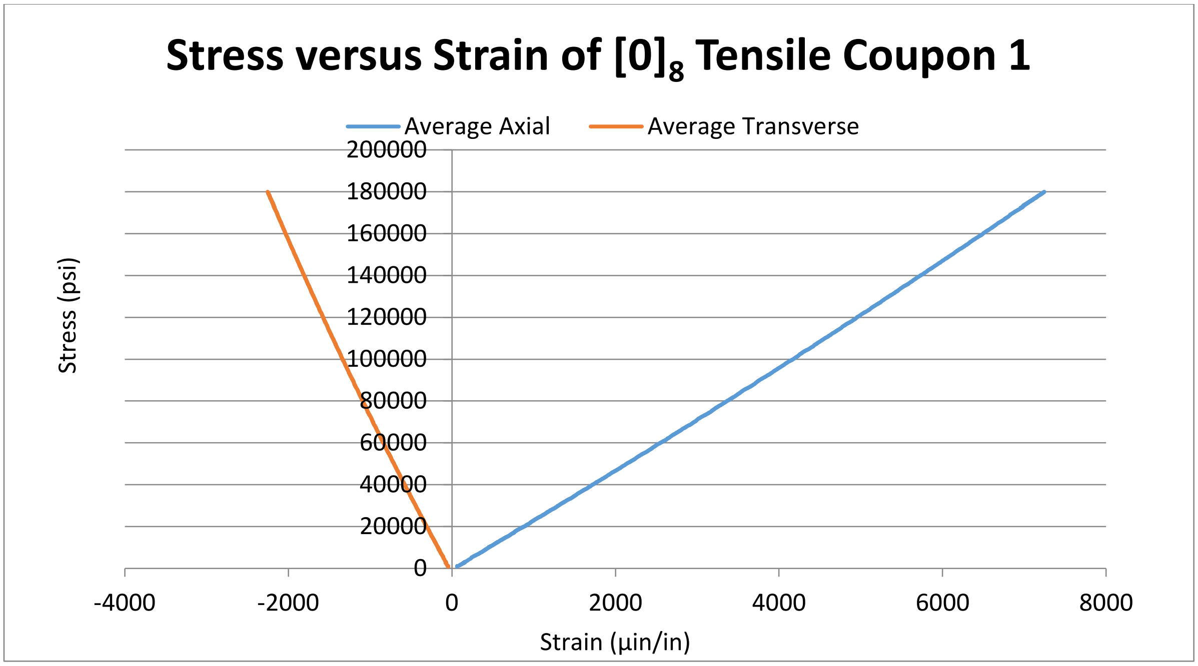

FIGURE 58: $[0]_8$ TENSILE COUPON 1

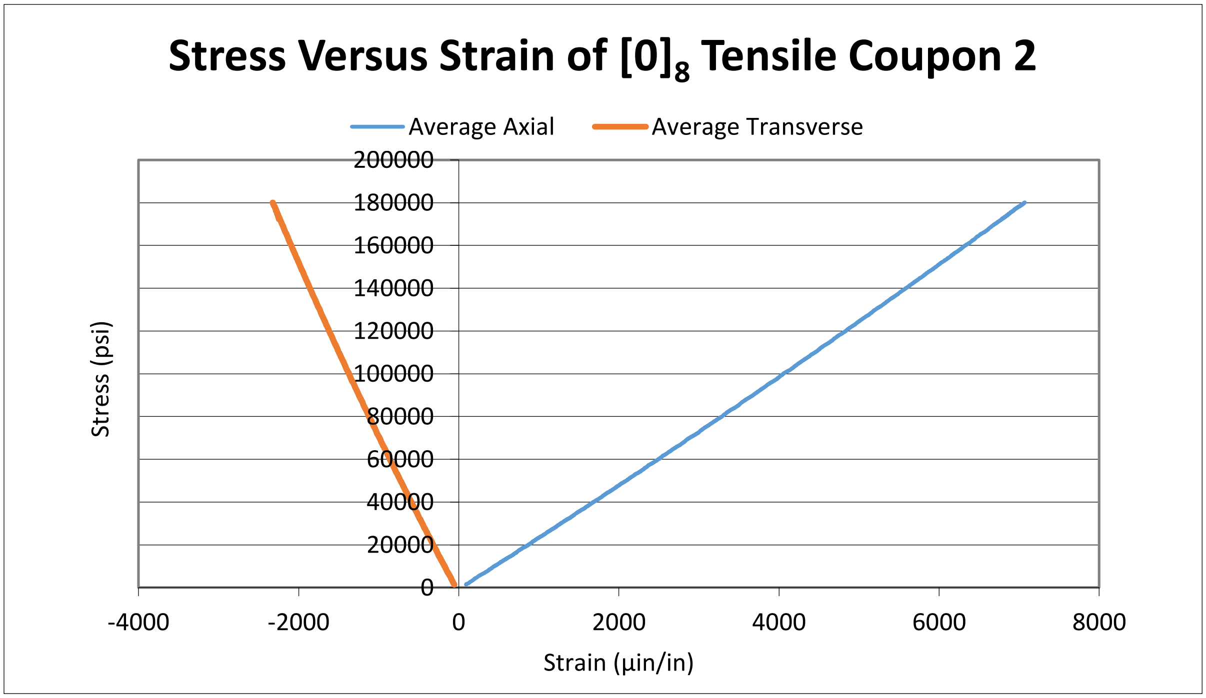

FIGURE 59: $[0]_8$ TENSILE COUPON 2

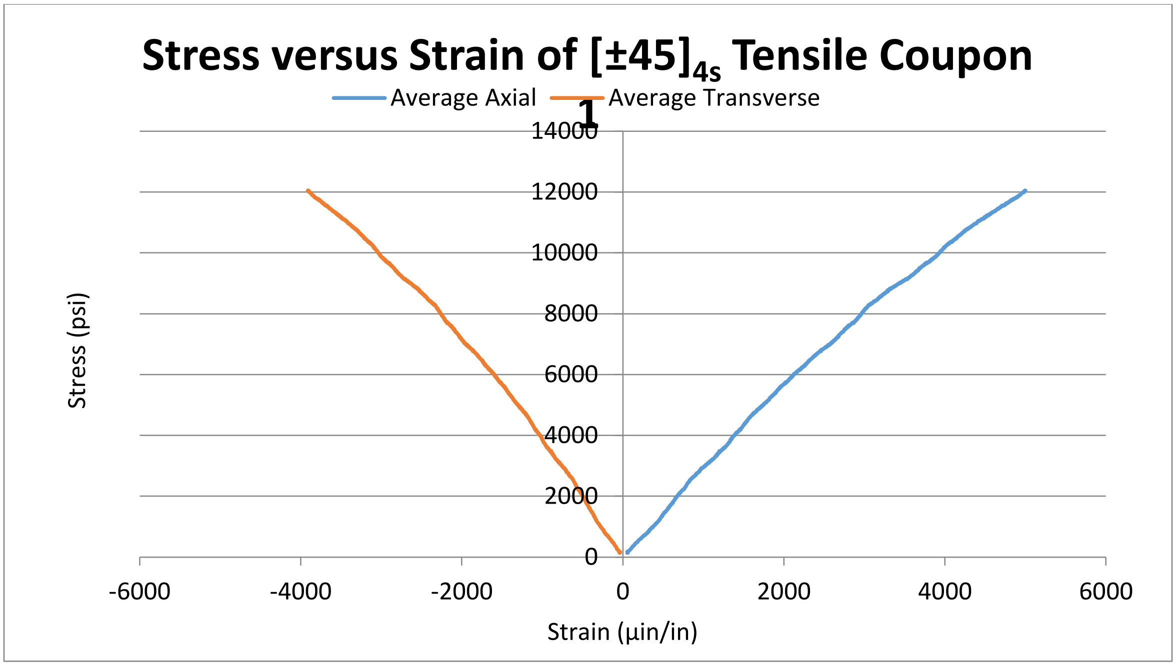

FIGURE 60: $[\pm45]_{4S}$ TENSILE COUPON 1

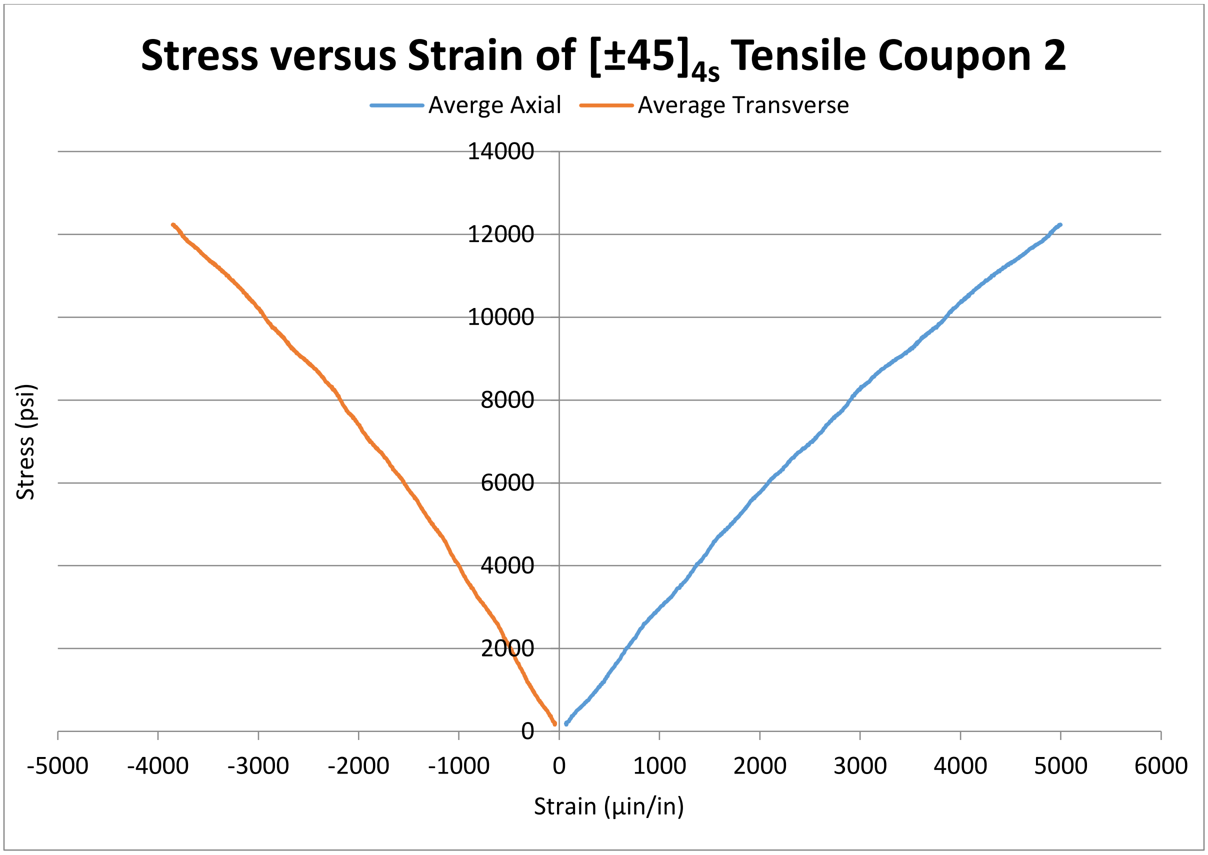

FIGURE 61: $[\pm45]_{4S}$ TENSILE COUPON 2

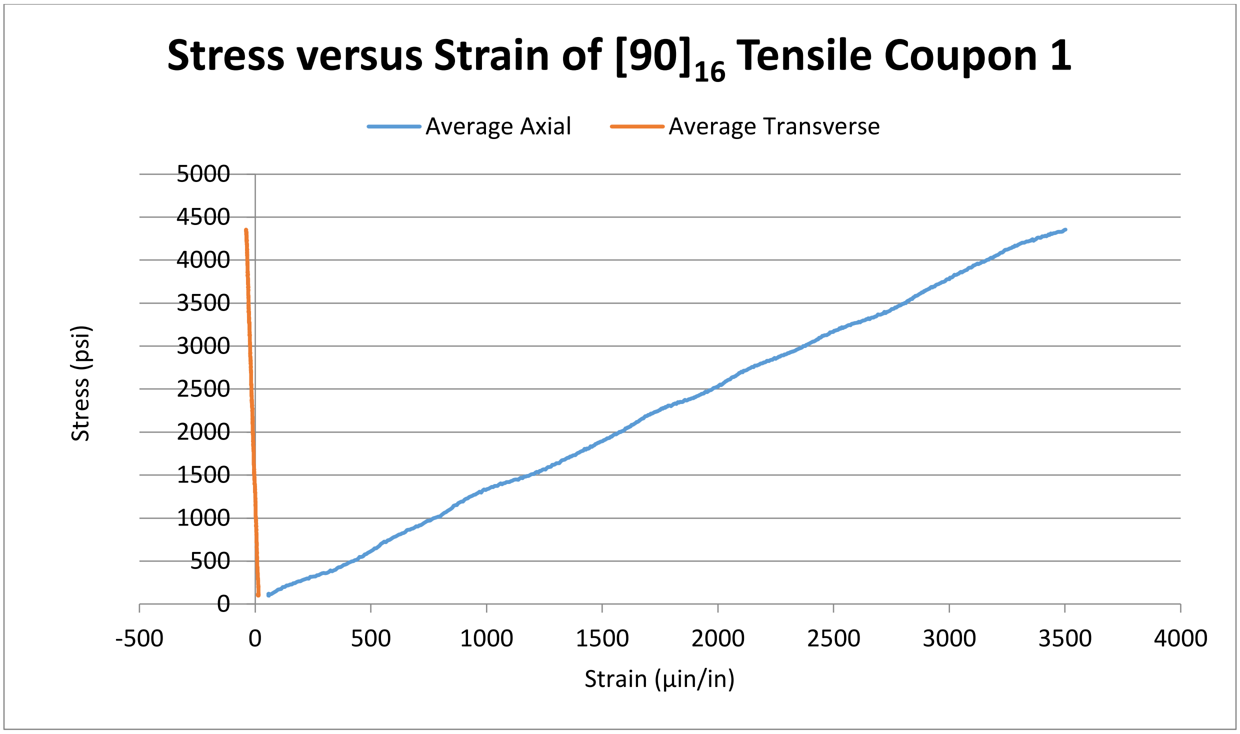

FIGURE 62: $[90]_{16}$ TENSILE COUPON 1

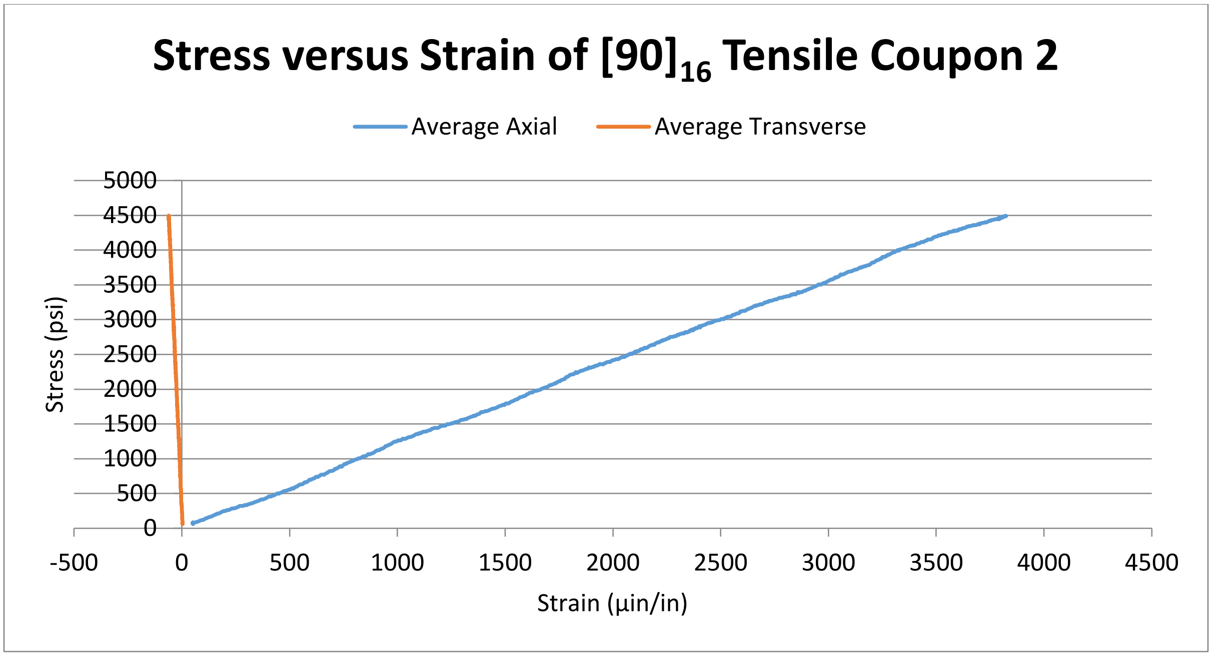

FIGURE 63: $[90]_{16}$ TENSILE COUPON 2

# Appendix D

Shows the results for the SPORTHO and ANSYS analyses for a panel cooling after cure and the resulting predicted buckling temperature.

**Table 11**: Shows results from the basic CLT analyses and the ANSYS analyses for the $[0]_{12}$ panel, run for comparison to validate the models created.

| Stacking Sequence | a (side length in the x-direction) | b (side length in the y-direction) | $T_{Buckle, SPORTHO}$ (°F) | $T_{Buckle, ANSYS}$ (°F) | % Error |
|---|---|---|---|---|---|
| $[0]_{12}$ | 12 | 12 | 108.5 | 108.17 | 0.3 |
| $[0]_{12}$ | 12 | 4 | 113.5 | 113.22 | 0.25 |
| $[0]_{12}$ | 12 | 3 | 128.6 | 128.36 | 0.19 |
| $[0]_{12}$ | 12 | 6 | 108.5 | 108.14 | 0.33 |
| $[0]_{12}$ | 4 | 12 | 360.5 | 353.55 | 1.93 |
| $[0]_{12}$ | 3 | 12 | 577.8 | 560.86 | 2.93 |
| $[0]_{12}$ | 6 | 12 | 203.1 | 200.97 | 1.05 |

**Table 12**: Shows results from the basic CLT analyses and the ANSYS analyses for the $[90]_{12}$ panel, run for comparison to validate the models created.

| Stacking Sequence | a (side length in the x-direction) | b (side length in the y-direction) | $T_{Buckle, SPORTHO}$ (°F) | $T_{Buckle, ANSYS}$ (°F) | % Error |
|---|---|---|---|---|---|
| $[90]_{12}$ | 12 | 12 | 108.5 | 108.17 | 0.3 |
| $[90]_{12}$ | 12 | 4 | 360.5 | 353.55 | 1.93 |
| $[90]_{12}$ | 12 | 3 | 577.8 | 560.86 | 2.93 |
| $[90]_{12}$ | 12 | 6 | 203.1 | 200.97 | 1.05 |
| $[90]_{12}$ | 4 | 12 | 113.5 | 113.22 | 0.25 |
| $[90]_{12}$ | 3 | 12 | 128.6 | 128.36 | 0.19 |
| $[90]_{12}$ | 6 | 12 | 108.5 | 108.14 | 0.33 |

**Table 13**: Shows results from the basic CLT analyses and the ANSYS analyses for the $[0_3/90_3]_s$ panel, run for comparison to validate the models created.

| Stacking Sequence | a (side length in the x-direction) | b (side length in the y-direction) | $T_{Buckle, SPORTHO}$ (°F) | $T_{Buckle, ANSYS}$ (°F) | % Error |
|---|---|---|---|---|---|
| $[0_3/90_3]_s$ | 12 | 12 | 145.4 | 144.5 | 0.62 |
| $[0_3/90_3]_s$ | 12 | 4 | 692.9 | 674.9 | 2.6 |
| $[0_3/90_3]_s$ | 12 | 3 | 1160.6 | 1116.3 | 3.8 |
| $[0_3/90_3]_s$ | 12 | 6 | 350.7 | 345.3 | 1.5 |
| $[0_3/90_3]_s$ | 4 | 12 | 257.2 | 254.7 | 0.97 |
| $[0_3/90_3]_s$ | 3 | 12 | 387.4 | 382.5 | 1.3 |
| $[0_3/90_3]_s$ | 6 | 12 | 171.6 | 170.34 | 0.73 |

**Table 14**: Shows results from the basic CLT analyses and the ANSYS analyses with offset poles for the $[0]_{12}$ panel, run for comparison to validate the models created.

| **Stacking Sequence** | **a (side length in the x-direction)** | **b (side length in the y-direction)** | $T_{Buckle, SPORTHO}$ **(°F)** | $T_{Buckle, ANSYS}$ **(°F)** | **% Error** |
|---|---|---|---|---|---|
| $[0]_{12}$ | 12 | 12 | 108.5 | 108.2 | 0.28 |
| $[0]_{12}$ | 12 | 4 | 113.5 | 352.9 | 2.11 |
| $[0]_{12}$ | 12 | 3 | 128.6 | 558.8 | 3.30 |
| $[0]_{12}$ | 12 | 6 | 108.5 | 200.8 | 1.13 |
| $[0]_{12}$ | 4 | 12 | 360.5 | 113.16 | 0.30 |
| $[0]_{12}$ | 3 | 12 | 577.8 | 128.3 | 0.27 |
| $[0]_{12}$ | 6 | 12 | 203.1 | 108.1 | 0.36 |

**Table 15**: Shows results from the basic CLT analyses and the ANSYS analyses with offset poles for the $[90]_{12}$ panel, run for comparison to validate the models created.

| **Stacking Sequence** | **a (side length in the x-direction)** | **b (side length in the y-direction)** | $T_{Buckle, SPORTHO}$ **(°F)** | $T_{Buckle, ANSYS}$ **(°F)** | **% Error** |
|---|---|---|---|---|---|
| $[90]_{12}$ | 12 | 12 | 108.5 | 108.2 | 0.28 |
| $[90]_{12}$ | 12 | 4 | 360.5 | 113.2 | 0.30 |
| $[90]_{12}$ | 12 | 3 | 577.8 | 128.3 | 0.27 |
| $[90]_{12}$ | 12 | 6 | 203.1 | 108.11 | 0.36 |
| $[90]_{12}$ | 4 | 12 | 113.5 | 352.9 | 2.11 |
| $[90]_{12}$ | 3 | 12 | 128.6 | 558.8 | 3.30 |
| $[90]_{12}$ | 6 | 12 | 108.5 | 200.8 | 1.13 |

**Table 16**: Shows results from the basic CLT analyses and the ANSYS analyses with offset poles for the $[0_3/90_3]_s$ panel, run for comparison to validate the models created.

| **Stacking Sequence** | **a (side length in the x-direction)** | **b (side length in the y-direction)** | $T_{Buckle, SPORTHO}$ **(°F)** | $T_{Buckle, ANSYS}$ **(°F)** | **% Error** |
|---|---|---|---|---|---|
| $[0_3/90_3]_s$ | 12 | 12 | 145.4 | 144.5 | 0.65 |
| $[0_3/90_3]_s$ | 12 | 4 | 692.9 | 674.1 | 2.70 |
| $[0_3/90_3]_s$ | 12 | 3 | 1160.6 | Did not converge | N/A |
| $[0_3/90_3]_s$ | 12 | 6 | 350.7 | 345.1 | 1.63 |
| $[0_3/90_3]_s$ | 4 | 12 | 257.2 | 254.5 | 1.05 |
| $[0_3/90_3]_s$ | 3 | 12 | 387.4 | 382.0 | 1.39 |
| $[0_3/90_3]_s$ | 6 | 12 | 171.6 | 170.3 | 0.78 |

# Appendix E

**Table 17**: Shows results from the ANSYS ACP analysis to recreate the Hyer solution for $[0_4/90_4]_T$ unsymmetric panels. In the z-deflection column, the minimum and maximum values were equivalent, which resulted in equivalent curvatures for the edges, but with opposite sign.

| Edge Length | Z-deflection | Curvature |
|---|---:|---:|
| 30 | ±0.36145 | ±0.003211 |
| 60 | ±1.4458 | ±0.003205 |
| 90 | ±3.2531 | ±0.003196 |
| 120 | ±5.7833 | ±0.003183 |
| 150 | ±9.0364 | ±0.003167 |
| 180 | ±13.012 | ±0.003147 |
| 210 | ±17.711 | ±0.003124 |
| 240 | ±23.133 | ±0.003098 |
| 270 | ±29.278 | ±0.003069 |
| 300 | ±36.145 | ±0.003037 |
| 3000 | ±3614.5 | ±0.000472 |

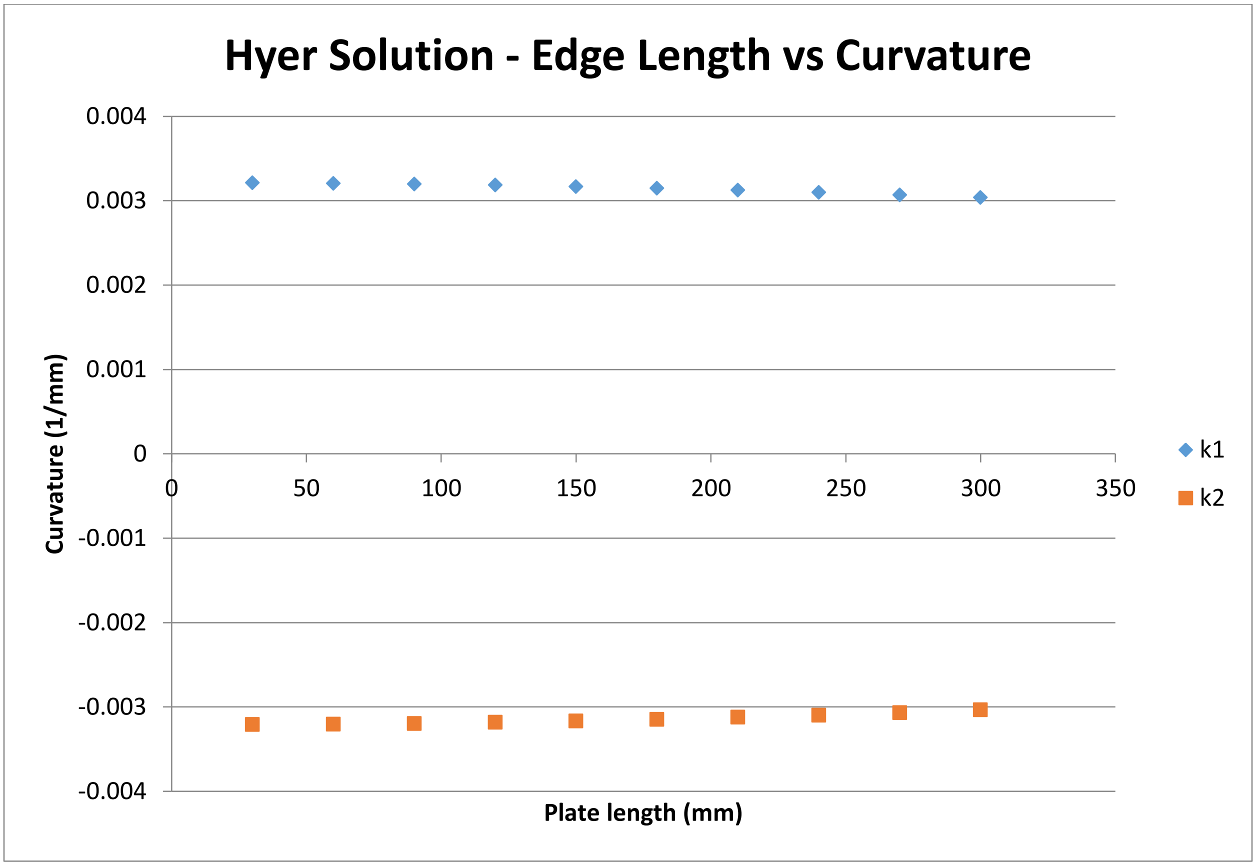

FIGURE 64: HYER SOLUTION EDGE VS CURVATURE